Università degli Studi di Padova

DIPARTIMENTO
DI INGEGNERIA
DELL'INFORMAZIONE

Università degli Studi di Padova

Dipartimento di Ingegneria dell'Informazione

Laurea Magistrale in Ingegneria Elettronica

Droop-Based Power Controller for Electronic Power Converters in Three-Phase Microgrids

Relatore: Ch.mo Prof. Tommaso Caldognetto

Laureando: Andrea Lauri

Matricola: 1225835

Anno Accademico 2021/22

14 aprile 2022

Contents

Acknowledgements

I want to dedicate this chapter to all the people who have accompanied me along this path and helped me to face the challenges that have arisen. First of all, I am extremely grateful to Prof. Tommaso Caldognetto: he offered me great support and shared with me priceless knowledge, always with extraordinary availability and humanity. Then, I would like to express my gratitude to all the people with whom I had the great pleasure to share my time in the Integrated Mechatronics Laboratory of the DTG department in Vicenza. The welcome I was shown from day one was great. I have been lucky enough to meet fantastic people, with whom I have had the pleasure of sharing wonderful moments. Among them, I am extremely grateful to Dr. Andrea Petucco, who with extraordinary patience, humanity, and great competence accompanied me in realizing how hard and treacherous reality is compared to expectations. I am also very grateful to Dr. Hossein Abedini, his knowledge and the great punctuality and meticulousness of his work have been decisive. I would also like to thank Prof. Paolo Mattavelli, to whom an important part of the credit goes for the high quality of the research activities carried out in the laboratory.

I would then like to continue by thanking Davide Fogagnolo and Enrico Sartori, fantastic classmates with whom to conclude the years of study. A big thank you to all my friends and to all the people I have met during these years, for the beautiful memories to treasure and the indispensable support provided.

I would like to give a special thanks to Chiara, who has been my strength and my most important support during these years. I would also like to thank all of Chiara's family, especially Laura and Simone, whose help has been truly invaluable.

Finally, I would like to thank my family, for making all of this possible and for the

unconditional support that has always been given to me.

Voglio dedicare questso capitolo a tutte le persone che mi hanno accompagnato lungo questo cammino e mi hanno aiutato ad affrontare le sfide che sono emerse. Innanzitutto, sono estremamente grato al prof. Tommaso Caldognetto: mi ha offerto grande supporto e ha condiviso con me impagabili conscenze, sempre con una straordinaria disponibilità e umanità. Vorrei, poi, esprimere la mia gratitudine verso tutte le persone con cui ho avuto il grande piacere di condividere il mio tempo nel Laboratorio Integrato di Meccatronica del dipartimento DTG di Vicenza. L'accoglienza che mi è stata dimostrata fin dal primo giorno è stata grande. Ho avuto la fortuna di conoscere persone fantastiche, con le quali ho avuto il piacere di condividere momenti bellissimi. Tra queste, sono estremamente grato al dott. Andrea Petucco, che con straordinaria pazienza, umanità e grande competenza mi ha accompagnato nel realizzare quanto più dura e insidiosa sia la realtà rispetto alle aspettative. Sono molto grato anche al dott. Hossein Abedini, le sue conoscenze e la grande puntualità e meticolosità del suo lavoro sono state decisive. Vorrei anche ringraziare il prof. Paolo Mattavelli, a cui va un'importante parte del merito per l'elevata qualità delle attività di ricerca che si svolgono nel laboratorio.
Vorrei poi continuare ringraziando Davide Fogagnolo ed Enrico Sartori, fantastici compagni di corso con cui concludere gli anni di studio. Un grande ringraziamento va poi a tutti i miei amici e a tutte le persone che ho potuto conoscere in questi anni, per i bei ricordi di cui fare tesoro e per l'indispensabile supporto fornito.
Un ringraziamento speciale lo vorrei riservare a Chiara, che in questi anni è stata la mia forza e il mio sostegno più importante. Vorrei ringraziare anche tutta la famiglia di Chiara, in particolare Laura e Simone, il cui aiuto è stato davvero prezioso.
Infine, vorrei ringraziare la mia famiglia, per aver reso possibile tutto questo e per il supporto incondizionato che mi è sempre stato dato.

Introduction

The electrical grid is currently evolving from a centralized to a decentralized paradigm. As opposed to past trends, in which power was generated in centralized plants and the electricity was distributed in a unidirectional manner to the final users, nowadays producers and consumers are typically considered as a unique entity, often referred to as *prosumers*. Distributed energy resources that characterize prosumers installations are spreading through the low-voltage electrical grids. Prosumers that can participate in the energy market by exploiting their power generation and control capabilities are gaining ground and are expected to assume a crucial role in the next decades.

Distributed energy storage will penetrate the low-voltage distribution scenario too. In this light, energy will be able to reach more and more areas, while delivery losses will diminish, thanks to local energy production. Moreover, the growing presence of energy storage systems will lower the peak demand of power and will allow choosing the best period to buy energy according to its price. This future scenario comes with many opportunities but, to fully exploit the benefits, new challenges should be tackled and new technologies need to be developed. These challenges considered herein are related to:

- resilience to variable power demand;
- reliability and continuity of service;
- optimal power quality distribution.

Flexible power control is necessary to effectively satisfy variable power demand, and it is essential to elevate the role of consumers to prosumers, allowing participation

in a transactive energy market. Fully exploiting the advantages of distributed energy resources means boosting the electrical grid reliability, allowing features that include the islanded operation of small portions of the grid in case of faults, thus ensuring service continuity. Lastly, the ability to inject and absorb reactive power can be exploited to obtain a better power factor and a more efficient electrical energy distribution.

In this thesis, a droop-based per-phase power controller is proposed. The control is studied considering a generic three-phase plus neutral network and analyzed and extended to the case of absence of the neutral connection. The technique features the possibility to fully control per-phase active and reactive power and allows smooth transitions to the islanded operation. Specifically, in this work, the technique is proposed and analyzed for use in three-wire networks taking into account all the limitations imposed by this particular connection.

The first of the following chapters starts reviewing classifications for grid-tied electronic power converters and the droop power control method, deepening the mentioned motivations behind such a power controller. Then, in Chapter 2, power flow in sinusoidal AC systems is also reviewed, to extend the droop analysis done before to a general case. In particular, power control possibilities and limitations in three-wires systems are analyzed. In Chapter 3 the control technique proposed in [1] is reviewed, and the modifications needed to operate in three-wires systems are pointed out. Chapter 4 shows a state-space representation of a three-phase inverter implementing this controller is proposed, providing guidelines for a design oriented to eigenvalues allocation. Finally, Chapter 5 shows and discusses simulations and experimental results.

Chapter 1

Literature review

To fully achieve what the future trends have to offer, electrical microgrids are growing more refined in measurements and control capabilities. Power control plays an essential role in overcoming the issues resulting in different scenarios. To allow active participation in energy transaction markets, it is necessary to be able to regulate the power exchanged with the grid regardless of its voltage and loading condition. In case of main grid failure, the devices composing the microgrid must be able to support the grid voltage to provide continuity of service. Finally, for the sake of power quality, the microgrid should be able to provide balance to an unbalanced electrical grid. In this chapter, the role of grid-forming and grid-following converters will be analyzed. Then, options proposed in the literature to tackle the aforementioned challenges are reviewed, and motivations for the proposed control system are discussed. Finally, the droop control method will be reviewed.

1.1 Grid-forming, grid-feeding and grid-supporting power converters

Electronic power converters connected to an AC grid can be classified depending on their operation mode [9]: this affects the reliability of the grid and determines whether a communication network is needed or not.

Grid-forming power converters

Grid-forming power converters are closed-loop controlled to emulate an ideal voltage source, given amplitude and phase/frequency references. Ideal voltage sources present zero output impedance: in practice, a voltage-controlled power converter presents a very low output impedance. They are employed to define and set the voltage behavior of an isolated system. Parallel connection of grid-forming converters is quite unusual: if theoretically possible through a common voltage reference signal, in practice, such a connection would lead to unacceptable circulating currents, due to voltage regulation mismatches. These mismatches can come from non-idealities in hardware components and in reference-signal propagation. Virtual impedances can be emulated by proper control to limit the effects of this problem, but too high impedances can be a disadvantage, thus leaving the problem quite unsolved in some situations, leaving circulating currents to unacceptable levels.

Grid-feeding power converters

Grid-feeding power converters are controlled to be able to operate in parallel with grid-forming and grid-supporting converters, and can not operate without the presence of at least one of such converters. Grid-feeding converters are closed-loop controlled to behave like an ideal current source, presenting in practice a high parallel output impedance. They can, ideally, be connected in parallel to voltage-source converters without affecting the voltage in the grid. In practice, there may be hierarchically higher control levels defining a limit to active power injection in the grid. Reactive power is regulated by referring to grid codes, to not distort the grid voltage and contribute to the power-quality increase.

Grid-supporting power converters

Grid-supporting power converters can either be current-controlled or voltage-controlled. Their control laws are implemented so that the converter emulates the behavior of a synchronous generator, which is intrinsically self-regulatory. Voltage amplitude de-

creases as reactive power is absorbed while grid frequency decreases as active power is injected: this droop characteristic is employed to sustain grid voltage in *islanded* grids, since it allows parallel connection of voltage-controlled grid-supporting converters, boosting the reliability of the grid in case of converter failure.

1.2 Control solutions currently available in literature

As previously discussed, grid-feeding power converters can't operate in absence of grid-forming or grid-supporting power converters, [10]. Even if sporting the advantage of total and per-phase power control, they are subject to the need for a power converter defining the grid voltage.

Regarding grid-supporting power converters, traditional droop control allows both grid-tied and island operation, [4], but static droop characteristic allows neither per-phase nor total power control. Another approach is proposed in [3], where angle instead of frequency is considered as drooped quantity. This control structure allows per-phase power control in four-wire systems but, because of the presence of a phase-locked loop, it is subject to the need for another converter defining the grid frequency and instantaneous phase. Traditional droop is employed with flexible droop characteristic in [7], allowing total active and reactive power tracking, and operation in both grid-tied and island operation, with a smooth transition toward the latter.

1.3 Droop power control

As the name suggests, droop control is based on allowing a small error on the grid parameters to regulate load sharing in the microgrid. Droop control opens the possibility of connecting in parallel voltage-controlled power converters, which will behave like grid-supporting power converters. Let us consider the islanded AC microgrid in Fig. 1-1. Usually, the impedance linking an electronic power converter (EPC) to the grid can be considered as an inductor in series with a resistor. Let us assume that

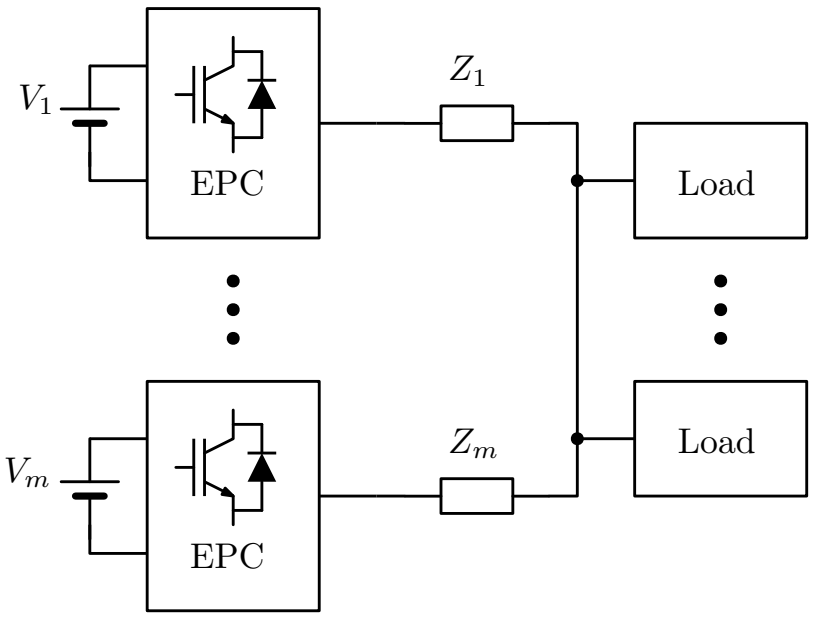

Figure 1-1: Microgrid composed of voltage-controlled electronic power converters and loads.

at the grid frequency the reactance of the impedance $j\omega L$ is much bigger than the resistance R. Even if not always true, this is still a reasonable assumption, as the inductive impedance can come from proper zero-level control of a power converter or a physical inductor. Anyway, in the next chapter, it will be shown how these results can be extended considering a generic impedance.

Assuming mainly inductive impedance, it can be shown (again, in the next chapter) that active and reactive power flow can be approximated by:

$$P \simeq \frac{V_g V_i}{\omega L} \Delta\varphi$$

$$Q \simeq \frac{V_g}{\omega L} \left(V_i - V_g\right)$$

where V_g is the grid nominal voltage, V_i is the EPC output voltage, ω is the grid angular frequency and $\Delta\varphi$ is the phase difference between EPC and grid voltage. In these conditions, it is clear that active power flow is influenced mainly by $\Delta\varphi$ while reactive power flow mainly by $\Delta V_i = V_i - V_g$.

At primary control level, by relaxing the grid voltage amplitude and frequency

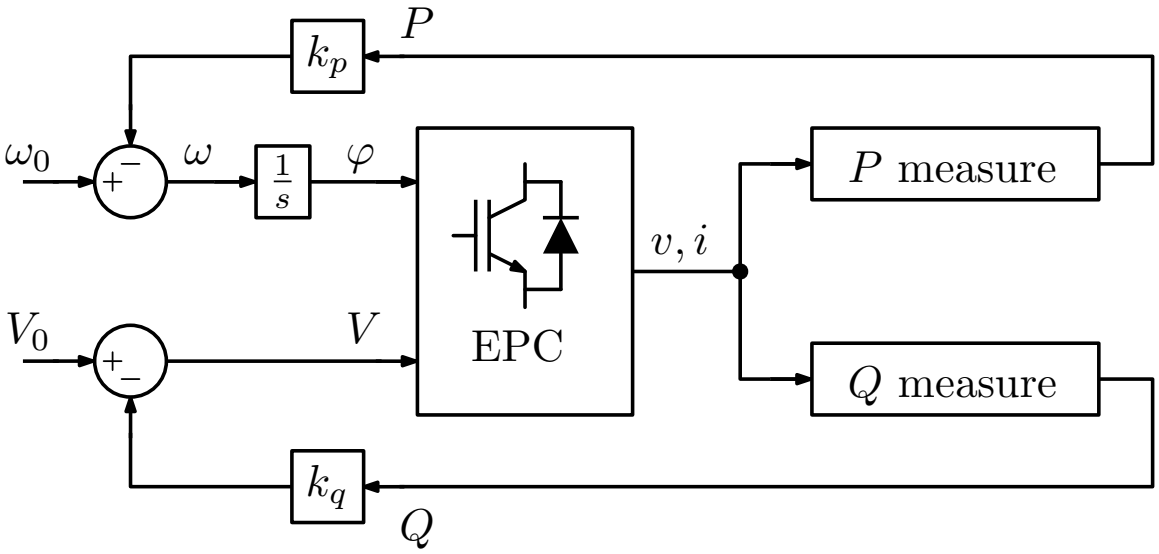

Figure 1-2: Primary level control scheme implementing droop control on a voltage-controlled power converter.

values around their nominal values, it is possible to impose the following laws:

$$\begin{aligned} \omega &= \omega_0 - k_p P \\ V &= V_0 - k_q Q \end{aligned} \tag{1.1}$$

Reactive power flow is controlled by varying the converter voltage amplitude, while active power flow is controlled by modifying the phase shift between converter and bus voltage, through an integral control of the converter frequency. The control scheme in Fig. 1-2 can be used at primary control level to implement the relations in (1.1).

Based on nominal power, which provides a worst-case scenario, droop coefficients k_p and k_q can be sized to keep frequency and amplitude errors within certain limits. Moreover, by basing the design on nominal power the converters will share the load power proportionally to their nominal power. In particular, the power load is shared *almost* proportionally if the following relation holds:

$$k_{p,1} S_1 = k_{p,2} S_2 = ... = k_{p,m} S_m$$

$$k_{q,1} S_1 = k_{q,2} S_2 = ... = k_{q,m} S_m$$

where S_i is the nominal power of the i-th converter. The "almost" is emphasized because while the statement holds for active power, things are different for reactive power. Let us consider a two converters microgrid, and let us consider the active power shared between the two:

$$\omega_1 = \omega_0 - k_{p,1}P_1, \quad \omega_2 = \omega_0 - k_{p,2}P_2$$

Then, since the equation $\omega_1 = \omega_2$ must be true (recalling that active power is function of phase-shift between voltages), and supposing $k_{p,1} \propto \frac{1}{S_1}$, $k_{p,2} \propto \frac{1}{S_2}$, then

$$k_{p,1}P_1 = k_{p,2}P_2$$

Finally, from the previous equations, it is possible to write:

$$P_2 = \frac{k_{p,1}}{k_{p,2}}P_1 = \frac{S_2}{S_1}P_1 \quad \Longrightarrow \quad P_1 = P_1\frac{P_1 + P_2}{P_1 + P_2} = P_{load}\frac{S_1}{S_1 + S_2}$$

$$P2 = P_{load} - P_1 = P_{load}\frac{S_2}{S_1 + S_2}$$

This result, represented in Fig. 1-3 (a), is obtained assuming that the frequency is the same among the converters, which is true at least in steady-state. For what concerns reactive power, the drooped quantity is the voltage, and in general it is not the same in the overall grid, since line impedances cause a voltage drop. If there is a difference between the converter voltage amplitudes, then the power is not shared proportionally even if the aforementioned relation holds, as shown in Fig. 1-3 (b).

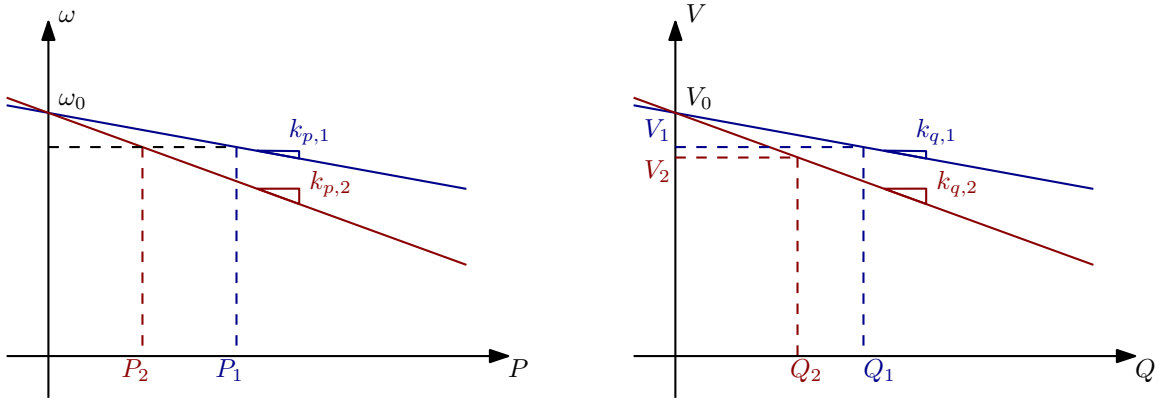

Figure 1-3: Droop characteristics for active power (a) and reactive power (b).

Chapter 2

Power-flow review in sinusoidal AC systems

In this chapter the power flow in sinusoidal systems will be reviewed, focusing on power flow analysis on an electronic power converter connected to an AC common bus. The analysis, starting from Thevenin's equivalent model, will derive equations for active and reactive power flow with generic coupling impedances in single-phase AC systems. Then the case of inductive impedance will be further analyzed, on three-phase four- and three-wires systems too.

2.1 Power flow with generic coupling impedance

Let us begin by considering a single-phase inverter connected to an AC common bus (grid). By making use of the Thevenin theorem, it is possible to model the inverter as a voltage generator with a proper series impedance. Similarly, it is possible to model the AC bus as a voltage generator with a proper series impedance, [11]. The equivalent circuit then is shown in Fig. 2-1, where $\bar{Z}$ is the overall impedance coupling the two generators, obtained by summing the two series impedances. Let be $\bar{V}_i = V_i \angle \varphi$, $\bar{Z} = Z \angle \theta$ and $\bar{V}_g = V_g \angle 0$. The complex power injected into the grid can be computed as

$$\dot{S} = P + jQ = \bar{V}_g \bar{I}^* \tag{2.1}$$

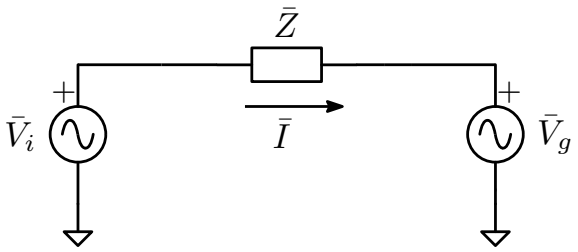

Figure 2-1: Thevenin model of a grid-connected voltage inverter.

where, according to the equivalent circuit, the current $\bar{I}$ is

$$\bar{I} = \frac{\bar{V}_i - \bar{V}_g}{\bar{Z}} = \frac{V_i}{Z}\angle(\varphi - \theta) - \frac{V_g}{Z}\angle(-\theta) \tag{2.2}$$

By combining (2.1) and (2.2) one obtains the expressions for the active power P and the reactive power Q:

$$\begin{aligned} P &= \frac{V_g}{Z}\left[(V_i\cos\varphi - V_g)\cos\theta + V_i\sin\theta\sin\varphi\right] \\ Q &= \frac{V_g}{Z}\left[(V_i\cos\varphi - V_g)\sin\theta - V_i\cos\theta\sin\varphi\right] \end{aligned} \tag{2.3}$$

Equation (2.3) relates active and reactive power flow with inverter voltage $\bar{V}_i$ amplitude and phase shift. In general, the impedance coupling the inverter and the grid can be modeled by taking into account an inductive component and a resistive component, namely:

$$\bar{Z} = Ze^{j\theta} = R + jX_L$$

where the angle $\theta = \arctan\left(\frac{X_L}{R}\right)$. If a purely resistive coupling impedance is considered, in which case the angle $\theta = 0$, the equations in (2.3) lead to:

$$\begin{aligned} P_{res} &= \frac{V_g}{Z}\left(V_i\cos\varphi - V_g\right) \\ Q_{res} &= \frac{V_g}{Z}V_i\sin\varphi \end{aligned} \tag{2.4}$$

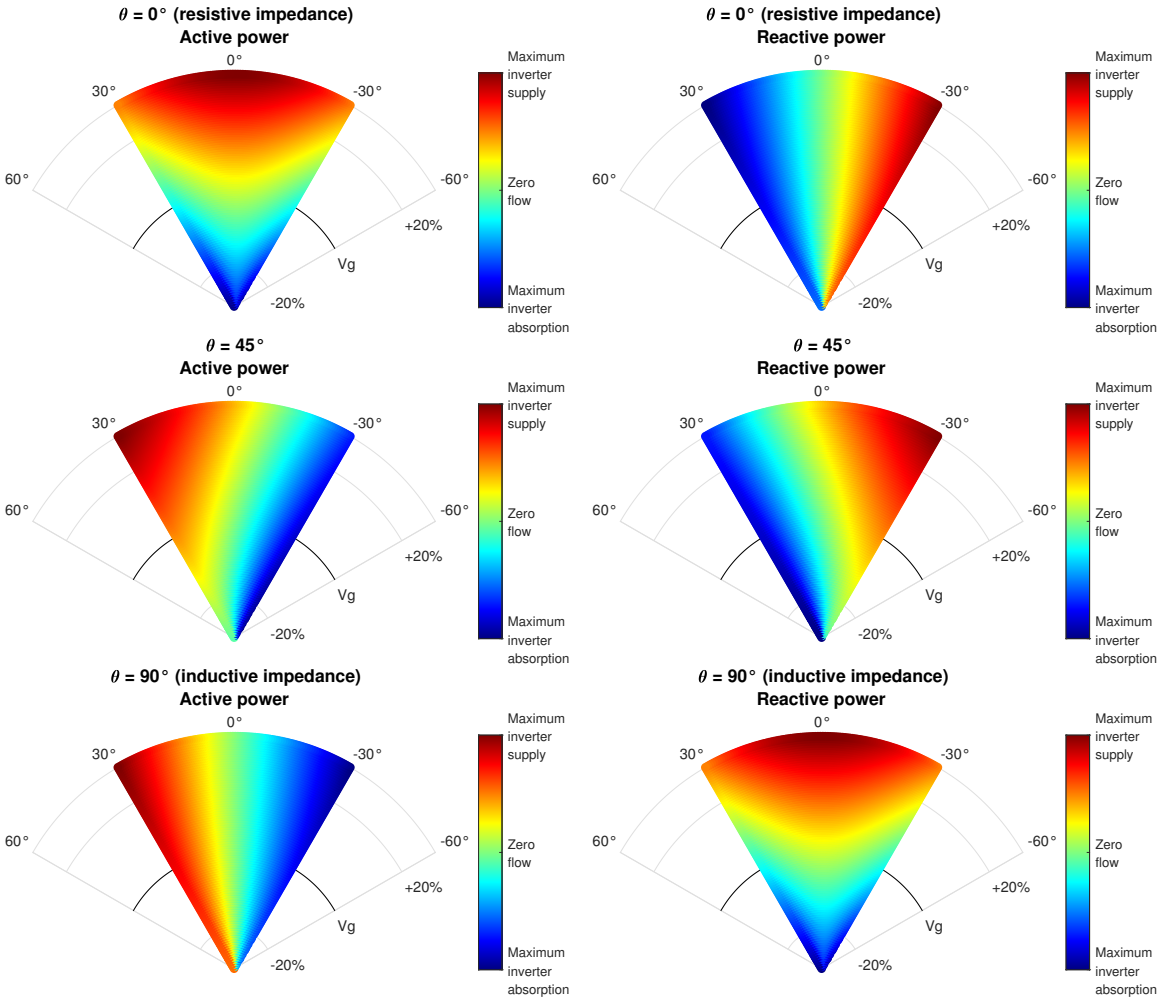

Figure 2-2: Polar diagrams showing power flow for various impedance angles θ. The radius of the plot corresponds to the amplitude variation of $\bar{V}_i$ with respect to $\bar{V}_g$, while the angle corresponds to the phase shift between $\bar{V}_i$ and $\bar{V}_g$.

In case of an inductive impedance, namely $\theta = 90°$, the equations in (2.3) can be written as:

$$\begin{aligned} P_{ind} &= \frac{V_g}{Z} V_i \sin\varphi \\ Q_{ind} &= \frac{V_g}{Z} \left(V_i \cos\varphi - V_g\right) \end{aligned} \tag{2.5}$$

To better understand these equations, polar diagrams are shown in Fig. 2-2. By looking at the two diagrams in the top row of Fig. 2-2, where a purely resistive coupling impedance is considered, it can be noticed that active power mainly depends on the inverter-voltage amplitude, while phase shift makes little to no difference in the power

flow. On the other side, reactive power mainly depends on inverter-voltage phase shift, while changing its amplitude makes little difference in power flow. On the contrary, by looking at the two diagrams on the bottom of Fig. 2-2, it is possible to conclude that active power flow mainly depends on voltage phase shift, while reactive power flow depends mainly on voltage amplitude. By looking at diagrams with different θ values, it is possible to recognize a rotation pattern in the power distribution along the polar chart. This can be explained by the fact that, by defining $P_0 \triangleq P_{res}$ and $Q_0 \triangleq Q_{res}$, which correspond to the power flow in a $\theta = 0$ impedance, the equation (2.3) can be written as:

$$\begin{bmatrix} P_\theta \\ Q_\theta \end{bmatrix} = \begin{bmatrix} \cos\theta & -\sin\theta \\ \sin\theta & \cos\theta \end{bmatrix} \cdot \begin{bmatrix} P_0 \\ Q_0 \end{bmatrix} \tag{2.6}$$

More generally, it is possible to write that:

$$\begin{bmatrix} P_{\theta+\Delta\theta} \\ Q_{\theta+\Delta\theta} \end{bmatrix} = \begin{bmatrix} \cos\Delta\theta & -\sin\Delta\theta \\ \sin\Delta\theta & \cos\Delta\theta \end{bmatrix} \cdot \begin{bmatrix} P_\theta \\ Q_\theta \end{bmatrix} \tag{2.7}$$

Equation (2.7) shows that by a simple rotation transformation it is possible to compute the power flow with a generic impedance. This should not be surprising, since (2.1) can be written as

$$\dot{S} = \bar{V}_g \left(\frac{\bar{V}_i - \bar{V}_g}{\bar{Z}} \right)^* = \bar{V}_g \left(\frac{\bar{V}_i - \bar{V}_g}{Z} \right)^* e^{j\theta}$$

This equation and (2.6) express the same relation, the former in $\mathbb{R}^2$ and the latter in the complex plane. Relation expressed in (2.7) is particularly useful when trying to control active and reactive power of such a system, where coupling impedance can be measured but is unknown from the start. In these situations, it is possible to design the power controller assuming purely resistive or purely inductive impedance, in which case it is possible to assume separation on the control actions of phase φ and amplitude V_i, and then close the loop transforming the measured power using the relation (2.7), [2].

Let us assume that the phase difference φ between the inverter and the grid voltages is small. This assumption is correct at least at the moment in which the inverter is connected to the grid, because its voltage reference is synchronized through, for example, a phase-locked loop. Then the equations in (2.3) can be simplified as:

$$\begin{aligned} P &\simeq \frac{V_g}{Z}\left[(V_i - V_g)\cos\theta + V_i\varphi\sin\theta\right] \\ Q &\simeq \frac{V_g}{Z}\left[(V_i - V_g)\sin\theta + V_i\varphi\cos\theta\right] \end{aligned} \tag{2.8}$$

2.2 Power flow with inductive coupling impedance

Let us now assume that the coupling impedance is mainly inductive. This hypothesis is usually verified, as it is possible to impose it with a proper zero-level control design, or employing physical inductors. Considering a single-phase inverter, as in Fig. 2-1, the equations representing the power flow (2.8) can be further simplified, since mainly inductive impedance means $\theta \simeq 90°$:

$$P \simeq \frac{V_i V_g}{\omega L}\varphi_i; \quad Q \simeq \frac{V_g}{\omega L}\left(V_i - V_g\right) \tag{2.9}$$

As shown in the bottom two diagrams in Fig. 2-2, active power mainly depends on phase shift, while reactive power depends mainly on amplitude difference, under the additional assumption that $V_i \simeq V_g$. The considerations and results derived from the model in Fig. 2-1 can be extended to three-phase inverters with neutral connection (four-wires three-phase inverters). Indeed, thanks to the presence of the neutral wire, there is no interdependence between phases a, b, c: the system behaves like three independent single-phase systems. Relations shown in (2.9) are thus valid phase-by-phase, namely:

$$P_x \simeq \frac{V_x V_g}{\omega L_x}\varphi_x; \quad Q_{\simeq}\frac{V_g}{\omega L_x}\left(V_x - V_g\right); \quad x = a, b, c \tag{2.10}$$

It is possible to regulate active and reactiv power flows of each phase independently. Power-flow equations get more complicated when considering a three-wire three-phase

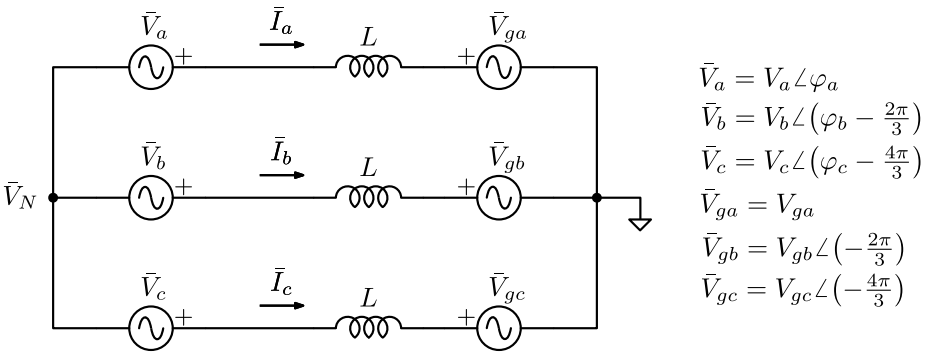

Figure 2-3: Three-phase inverter, without neutral wire, connected to the grid.

inverter, without a neutral connection. Let us consider the system in Fig. 2-3, representing a three-wires three-phase inverter connected to the grid. Using Kirchhoff voltage law (KVL) and Kirchhoff current law (KCL), one can write the following system of equations:

$$\begin{cases} \bar{V}_n + \bar{V}_a - j\omega L \bar{I}_a - \bar{V}_{ga} = 0 \\ \bar{V}_n + \bar{V}_b - j\omega L \bar{I}_b - \bar{V}_{gb} = 0 \\ \bar{V}_n + \bar{V}_c - j\omega L \bar{I}_c - \bar{V}_{gc} = 0 \\ \bar{I}_a + \bar{I}_b + \bar{I}_c = 0 \end{cases} \tag{2.11}$$

One can easily find the expression of the neutral point votlage $\bar{V}_n$ by summing the first three equations, and comparing the result with the fourth one:

$$\bar{V}_n = \frac{\bar{V}_a + \bar{V}_b + \bar{V}_c}{3} \tag{2.12}$$

At this point it is easy to write the expression for each of the three currents:

$$\begin{cases} \bar{I}_a = \dfrac{\bar{V}_a - \bar{V}_{ga} - \bar{V}_n}{3} = \dfrac{1}{j\omega L}\left[+\dfrac{2}{3}\bar{V}_a - \dfrac{1}{3}\bar{V}_b - \dfrac{1}{3}\bar{V}_c - \bar{V}_{ga}\right] \\ \bar{I}_b = \dfrac{\bar{V}_b - \bar{V}_{gb} - \bar{V}_n}{3} = \dfrac{1}{j\omega L}\left[-\dfrac{1}{3}\bar{V}_a + \dfrac{2}{3}\bar{V}_b - \dfrac{1}{3}\bar{V}_c - \bar{V}_{gb}\right] \\ \bar{I}_c = \dfrac{\bar{V}_c - \bar{V}_{gc} - \bar{V}_n}{3} = \dfrac{1}{j\omega L}\left[-\dfrac{1}{3}\bar{V}_a - \dfrac{1}{3}\bar{V}_b + \dfrac{2}{3}\bar{V}_c - \bar{V}_{gc}\right] \end{cases} \tag{2.13}$$

The expressions of currents in (2.13) highlight the main difference with respect to four-wire systems: each current is influenced by quantities belonging to all three phases a, b, c. By removing the neutral connection, one obtains that independence between phases a, b, c does not hold anymore. Complex power absorbed by a generic phase of the grid can be computed as:

$$\dot{S}_x = P_x + jQ_x = \bar{V}_{gx}\bar{I}_x^* \tag{2.14}$$

As an example, the calculations for the complex power of phase a are reported. Substituting the phasor expressions of Figg. 2-3, 2.13 in (2.1), one obtains:

$$\dot{S}_a = \bar{V}_{ga}\bar{I}_a^* = -\frac{\bar{V}_{ga}}{j\omega L}\left[\frac{2}{3}V_a e^{j\varphi_a} - \frac{1}{3}V_b e^{j\left(\varphi_b - \frac{2\pi}{3}\right)} - \frac{1}{3}V_c e^{j\left(\varphi_c - \frac{4\pi}{3}\right)}\right]^*$$

Rewriting the phasors in algebric form, namely $re^{j\varphi} = r\,(cos\,\varphi + j\,sin\,\varphi)$, and by linearizing the sinusoidal terms around $\varphi_x = 0$, one obtains:

$$\begin{aligned}\dot{S}_a = P_a + jQ_a \simeq \frac{2}{3}\frac{V_{ga}V_a}{\omega L}\varphi_a + \frac{1}{6}\frac{V_{ga}V_b}{\omega L}\varphi_b + \frac{1}{6}\frac{V_{ga}V_c}{\omega L}\varphi_c + \frac{\sqrt{3}}{6}\frac{V_{ga}}{\omega L}\left(\Delta V_b - \Delta V_c\right) + \\ + j\left[\frac{2}{3}\frac{V_{ga}}{\omega L}\Delta V_a + \frac{1}{6}\frac{V_{ga}}{\omega L}\Delta V_b + \frac{1}{6}\frac{V_{ga}}{\omega L}\Delta V_c - \frac{\sqrt{3}}{6}\frac{V_{ga}V_b}{\omega L}\varphi_b + \frac{\sqrt{3}}{6}\frac{V_{ga}V_c}{\omega L}\varphi_c\right]\end{aligned}$$

By noticing that $V_{gx}V_x = V_{gx}\left(V_{gx} + \Delta V_x\right) \simeq V_{gx}^2$, and under the assumption $V_{ga} = V_{gb} = V_{gc} = V_g$ then it is worthwile defining the following terms:

$$\gamma_p \triangleq \frac{V_g^2}{\omega L}; \quad \gamma_q \triangleq \frac{V_g}{\omega L} \tag{2.15}$$

Observing the expression of complex power for phase a, it is clear that it depends on all six variables $\varphi_{a,b,c}$, $\Delta V_{a,b,c}$. Moreover, active power P_a and reactive power Q_a are *linear combinations* of these six variables, once defined (2.15). By carrying out calculations also for complex powers of phase b and c one gets similar expressions, namely linear combinations of the same six variables. Hence, it is possible to inspect the regulation possibilities by studying the rank of the associated linear transforma-

tion. One can collect the equations for $P_{a,b,c}$, $Q_{a,b,c}$ and write them in matrix form, obtaining:

$$\begin{bmatrix} P_a \\ P_b \\ P_c \\ Q_a \\ Q_b \\ Q_c \end{bmatrix} = \underbrace{\frac{1}{6}\begin{bmatrix} 4\gamma_p & \gamma_p & \gamma_p & 0 & \sqrt{3}\gamma_q & -\sqrt{3}\gamma_q \\ \gamma_p & 4\gamma_p & \gamma_p & -\sqrt{3}\gamma_q & 0 & \sqrt{3}\gamma_q \\ \gamma_p & \gamma_p & 4\gamma_p & \sqrt{3}\gamma_q & -\sqrt{3}\gamma_q & 0 \\ 0 & -\sqrt{3}\gamma_p & \sqrt{3}\gamma_p & 4\gamma_q & \gamma_q & \gamma_q \\ \sqrt{3}\gamma_p & 0 & -\sqrt{3}\gamma_p & \gamma_q & 4\gamma_q & \gamma_q \\ -\sqrt{3}\gamma_p & \sqrt{3}\gamma_p & 0 & \gamma_q & \gamma_q & 4\gamma_q \end{bmatrix}}_{M} \cdot \begin{bmatrix} \varphi_a \\ \varphi_b \\ \varphi_c \\ \Delta V_a \\ \Delta V_b \\ \Delta V_c \end{bmatrix} \tag{2.16}$$

The rank of $M \in \mathbb{R}^{6\times 6}$ is $rank\,(M) = 4$: this means that it is not possible to arbitrarily set the values of $P_{a,b,c}$ e $Q_{a,b,c}$. The lack of a neutral wire connection not only creates phase-interdependence but also makes it physically impossible to arbitrarily set the active and reactive power of each phase.

Despite these disadvantages, the possibilities allowed by this system are still interesting. In (2.16) one can notice that by taking whichever subset of four rows in the six composing matrix M, one always gets a linear transformation which has rank 4. Therefore, it is possible to choose any four out of six terms $P_{a,b,c}$, $Q_{a,b,c}$ and arbitrarily set their value. For example, one can choose to regulate P_a, P_b, Q_a and Q_b: given a target value for these variables, there always exist a combination of $\varphi_{a,b,c}$ and $\Delta V_{a,b,c}$ such that the given target value is obtained. Furthermore, regulation possibilities are not limited to these. One may be interested in regulating, for example, the active power for all three phases a, b, c: then by choosing to regulate reactive power only on a single phase, one loses control on total reactive power. It can be shown, however, that control of total reactive power $Q_{3\varphi}$ is possible together with control of $P_{a,b,c}$ quantities. In fact, by summing the last three equations in (2.16) one obtains the expression of total reactive power, which can be collected in matrix form together

with $P_{a,b,c}$ expression, leading to:

$$\begin{bmatrix} P_a \\ P_b \\ P_c \\ Q_{3\varphi} \end{bmatrix} = \frac{1}{6} \begin{bmatrix} 4\gamma_p & \gamma_p & \gamma_p & 0 & \sqrt{3}\gamma_q & -\sqrt{3}\gamma_q \\ \gamma_p & 4\gamma_p & \gamma_p & -\sqrt{3}\gamma_q & 0 & \sqrt{3}\gamma_q \\ \gamma_p & \gamma_p & 4\gamma_p & \sqrt{3}\gamma_q & -\sqrt{3}\gamma_q & 0 \\ 0 & 0 & 0 & 6\gamma_q & 6\gamma_q & 6\gamma_q \end{bmatrix} \cdot \begin{bmatrix} \varphi_a \\ \varphi_b \\ \varphi_c \\ \Delta V_a \\ \Delta V_b \\ \Delta V_c \end{bmatrix} \tag{2.17}$$

The rank of the 4×6 matrix in (2.17) is still 4, so it is possible to arbitrarily set the values of $P_{a,b,c}$ and $Q_{3\varphi}$. Moreover, it is possible to obtain this same regulation possibility without the need for three different amplitude values $\Delta V_{a,b,c}$: one can simply impose

$$V_a = V_b = V_c = V \quad \Longrightarrow \quad \Delta V_a = \Delta V_b = \Delta V_c = \Delta V$$

obtaining the following transformation:

$$\begin{bmatrix} P_a \\ P_b \\ P_c \\ Q_{3\varphi} \end{bmatrix} = \frac{1}{6} \begin{bmatrix} 4\gamma_p & \gamma_p & \gamma_p & 0 \\ \gamma_p & 4\gamma_p & \gamma_p & 0 \\ \gamma_p & \gamma_p & 4\gamma_p & 0 \\ 0 & 0 & 0 & 18\gamma_q \end{bmatrix} \cdot \begin{bmatrix} \varphi_a \\ \varphi_b \\ \varphi_c \\ \Delta V \end{bmatrix} \tag{2.18}$$

which clearly has rank 4. It is important to remember that the transformation describing the (linearized) behaviour of the system is still (2.16): the description in (2.18) and in (2.17) is simply neglecting the phase-by-phase reactive power and considering only total reactive power $Q_{3\varphi}$.

Chapter 3

Per-phase power controller overview

In this chapter, the per-phase power controller proposed in [1] is reviewed, in both its working principle and design. Some modifications are carried out on the controller scheme, to comply with three-wire connection limitations. Finally, a modified version of the controller structure is shown, allowing the control of active and reactive power in two among three phases of the inverter.

3.1 Per-phase power-control in 3ϕ four-wires systems

In [1] a per-phase power controller has been proposed. It is meant for three-phase inverters with a neutral connection. As seen in Section 2.2, per-phase active and reactive power can be arbitrarily regulated in this case, in compliance with inverter power rating. The controller is composed of a synchronization loop, a per-phase active-power loop a and per-phase reactive-power loop, as shown in Fig. 3-1.

During grid-tied operation, in which case power control is possible, the synchronization loop regulates total active power by modifying inverter instantaneous phase $\varphi_{3\phi}$. This loop is responsible for synchronizing the inverter instantaneous phase with the grid instantaneous phase, with a phase shift, according to total active power reference $P_{3\phi}^{ref}$. Then the per-phase active-power loop furtherly adjusts the per-phase shifts, to achieve the correct per-phase power tracking. It is important to notice here that the per-phase active-power loop can regulate also total active power, or better

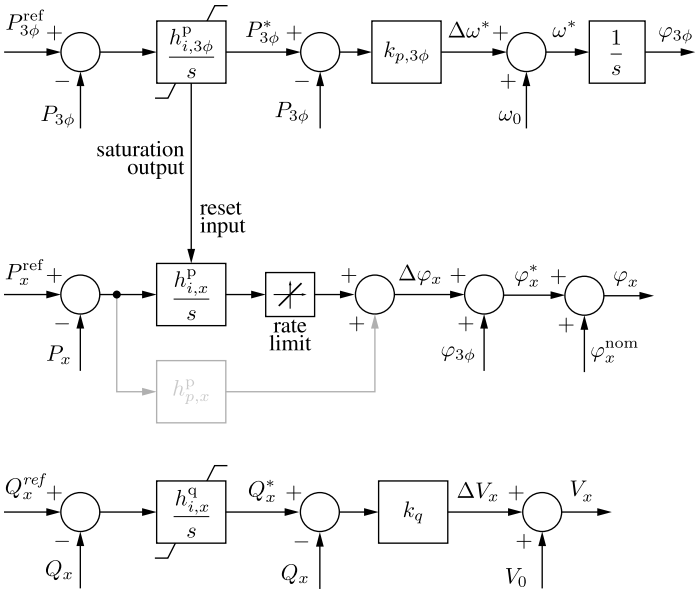

(a) Block scheme of the proposed controller.

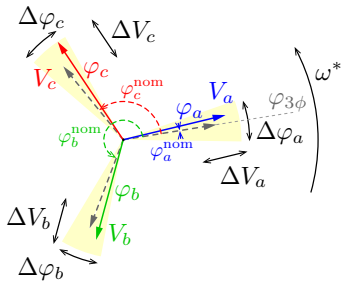

(b) Diagram explaining the considered angular quantities.

Figure 3-1: Control scheme.

said, total active power depends on the dynamics of both loops. Depending on the application, this can be a problem: for example if one wants total and per-phase power regulation with distinct and specific dynamics. The solutions will be discussed further on. Finally, the per-phase reactive-power loop sets the output voltage amplitude according to the per-phase reactive-power references.

When the grid is disconnected, output power control is no more possible, as the output power is now imposed by the load. Integral outputs in the system start growing positive or negative, depending on the reference value. Once the saturation level is reached for the synchronization loop, the per-phase active-power loop becomes disabled, so that total active power is regulated according to a P-f droop law:

$$\omega^* = \omega_0 + k_{p,3\phi}\left(P^*_{3\phi} - P_{3\phi}\right) \tag{3.1}$$

where $P^*_{3\phi}$ is constant and equal to either the higher or lower saturation level of the corresponding integrator. Similarly, when saturation is reached for the integrator in

the reactive-power control loop, the reactive power is regulated by a Q-V droop law:

$$V_x = V_0 + k_q \left(Q_x^* - Q_x\right) \tag{3.2}$$

where Q^* is either higher or lower saturation level of the corresponding integrator.

3.1.1 Controller design

Let us briefly review a possible design method for the regulator in [1]. The design should start from the droop operation of the controller: one needs to set the droop coefficients and the saturation levels for the integrators. An effective way to do that is the procedure in [7], which is reported here. Let us assume that our inverter can either supply or absorb nominal power S_N, and consider the P-f droop law in (3.1): for a fixed $P_{3\phi}^*$, there is a range of variation for angular frequency which depends on the total active power flow, and whose length can be computed as $\Delta\omega_{max} = 2k_{p,3\phi}S_N$. Similarly, for the Q-V droop law one can compute $\Delta V_{max} = 2k_q S_N/3$. One can then set the droop coefficients considering the maximum deviation allowed from the nominal value, with fixed P^* and Q^* values.

$$k_{p,3\phi} = \frac{\Delta\omega_g^{max}}{2S_{max}}; \quad k_q = \frac{3}{2}\frac{\Delta V_x^{max}}{S_{max}} \tag{3.3}$$

To determine the proper saturation levels for the integrators, one should consider maximum and minimum power values to be tracked as long as grid frequency and voltage deviations from nominal values. Let us stick with the assumption of S_N being the maximum power either absorbed or supplied by the inverter, and let us consider the P-f droop law in (3.1): one can write

$$P_{3\phi}^* = P_{3\phi} + \frac{\omega^* - \omega_0}{k_{p,3\phi}}$$

Maximum and minimum values for $P^*_{3\phi}$ are reached, respectively, for maximum and minimum output power and grid frequency. Then:

$$P_{3\phi}^{*max,min} = \pm S_N + \frac{\omega_{max,min} - \omega_0}{k_{p,3\phi}} \tag{3.4}$$

Let us now consider the Q-V droop law in (3.2): with similar considerations as before, one can write:

$$Q_x^* = Q_x + \frac{V - V_0}{k_q}$$

and then obtain saturation values as

$$Q_x^{*max,min} = \pm S_N + \frac{V_{max,min} - V_0}{k_q} \tag{3.5}$$

Regarding the Q-V droop law, since voltage may be different along the grid, saturation levels may need to be extended to allow full-range reactive power tracking.

Now that droop coefficients $k_{p,3\phi}$ and k_q are defined, one can design the dynamics of the regulation loops. As previously pointed out, both the synchronization loop and the per-phase active-power loop contribute to regulating total active power. This peculiarity can, however, be a problem in some cases: for example if one wants to set different and specific dynamics for total and per-phase active powers. A possible solution is to exploit *time-scale separation* and design the per-phase active power loop much slower than the synchronization loop. Another solution would be to pre-transform the quantities $P_x^{ref} - P_x$ to remove the homopolar component. This latter solution will be analyzed later on when the application of this controller to a three-phase system without a neutral wire will be considered. For now, it is sufficient to assume that the dynamics of the two loops are separated, and total active power is regulated only by the synchronization loop. Under this assumption, the integral gain of the synchronization loop $h^{\mathrm{p}}_{i,3\phi}$ can be designed by considering the following uncompensated loop gain:

$$T_{p,3\phi} = \frac{3\gamma_p k_{p,3\phi}\frac{1}{s}}{1 + 3\gamma_p k_{p,3\phi}\frac{1}{s}} = \frac{1}{1 + {}^{s}\!/_{\omega_p}}$$

where $\omega_p = 3\gamma_p k_{p,3\phi}$ and $\gamma_p = \frac{V_g^2}{\omega L}$. while the loop gain relevant for the design of the per-phase active-power loop integral gain $h_{i,x}^{\mathrm{p}}$ is simply a proportional term:

$$T_{p,x} = \frac{V_g^2}{\omega L} = \gamma_p$$

Finally, the integral gain of the per-phase reactive-power loop $h_{i,x}^{\mathrm{q}}$ has to be designed considering the following loop gain, which still is a proportional term:

$$T_{q,x} = \frac{1}{1 + \frac{1}{\gamma_q k_q}}$$

3.2 Per-phase power control in 3ϕ three-wires systems

The controller proposed in [1] can also be used in three-phase inverters without a neutral connection. Some modifications need to be done, in light of the analysis carried out in Section 2.2. The controller must be modified so that it complies with the possibilities allowed by (2.16). As discussed in that section, the allowed possibilities are various. This thesis focuses on the possibility of regulating active power $P_{a,b,c}$ for all the three phases of the inverter, while only total reactive power $Q_{3\phi}$ is regulated. At the end of the section, another configuration is shown, which allows regulating active and reactive power in two phases of the three-phase system, leaving these quantities free to vary for the third phase.

3.2.1 Control of P_a, P_b, P_c and $Q_{3\phi}$

The controller structure needs to be adapted to achieve the desired power tracking behavior. Some modifications are carried out with respect to the block scheme proposed in [1]: the goal here is to control P_a, P_b, P_c and $Q_{3\phi}$. The synchronization loop and the per-phase active-power loop can be left as they are, since active power is regulated in the same way. The reactive-power loop, instead, should be closed around

the total reactive power: it is sufficient to feed the controller with $Q_{3\phi}^{ref} = \sum Q_x^{ref}$ and $Q_{3\phi} = \sum Q_x$, where $x = a, b, c$. The reactive regulator generates a single voltage amplitude signal, which is the same for all the three phases of the system. Another major modification regards the generated voltage waveforms. In a system without a neutral connection, the term $\bar{V}_n$ appears in the mesh equations (KVL) of each phase, as in (2.11), and it corresponds to the homopolar component of the generated voltages, according to (2.12). This homopolar component can lead to voltage and power tracking errors in the control system. Indeed, if we consider a generic voltage source inverter, the controller is trying to regulate the average potential of the switching node with respect to the DC-source midpoint voltage: this latter is a theoretically constant voltage equal to zero *only* if there is no homopolar component in the generated voltage. A possible solution is to exploit a transformation matrix to remove this undesired component from the voltage references fed to the controller:

$$\begin{bmatrix} \bar{V}'_a \\ \bar{V}'_b \\ \bar{V}'_c \end{bmatrix} = \begin{bmatrix} \frac{2}{3} & -\frac{1}{3} & -\frac{1}{3} \\ -\frac{1}{3} & \frac{2}{3} & -\frac{1}{3} \\ -\frac{1}{3} & -\frac{1}{3} & \frac{2}{3} \end{bmatrix} \cdot \begin{bmatrix} \bar{V}_a \\ \bar{V}_b \\ \bar{V}_c \end{bmatrix} \tag{3.6}$$

The transformation in (3.6) does not modify the nature of the relations in (2.11), (2.12) and (2.13). In fact, by substituting (3.6) in (2.11), one still obtains an expression like (2.13), leading to the very same relation as in (2.16).

In Section 3.1.1 the problem of the interaction between the synchronization loop and the per-phase active-power loop was mentioned. In particular, the per-phase active-power loop interferes in the regulation of the total active power, and this can be a problem in some applications. The definition of a specific dynamical behavior can become a difficult task because of this phenomenon. Moreover, this lack of clearness in the loop roles can prevent the definition of safety conditions and safety systems. The source of this phenomenon is the fact that nothing prevents the per-phase loop from regulating total active power, since it simply reacts to the per-phase power-tracking error. A simple solution was proposed in [1]: designing the per-phase loop much slower than the synchronization loop, one obtains that the contribution given

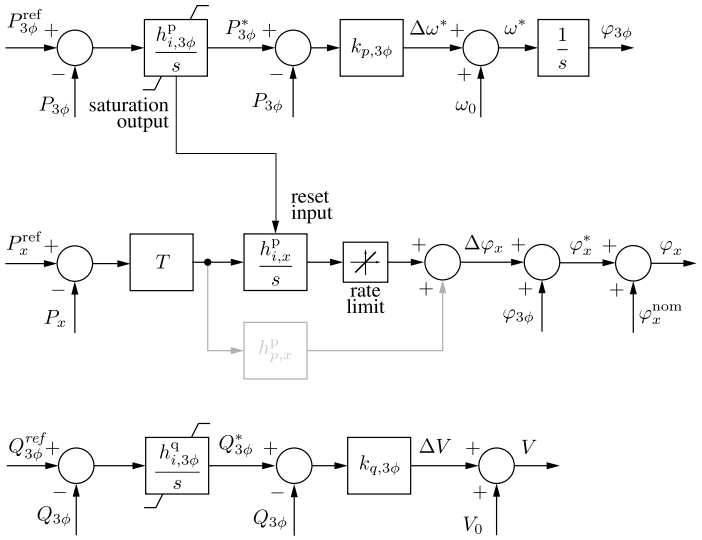

Figure 3-2: Block scheme of the controller allowing control of per-phase active power and total reactive power.

by the per-phase loop to the total active power regulation is negligible, because of its slow dynamics compared to the ones of the synchronization loop. The main problem with this is the presence of a pole in the uncompensated loop gain $T_{p,3\phi}$, which limits the maximum obtainable bandwidth. The performances obtained by an even slower per-phase loop are quite limited. A cleaner solution is found in feeding the per-phase active-power regulator with pre-transformed power-tracking errors. Indeed, the homopolar component in these tracking errors corresponds to the total active power, and removing this component from these error signals prevents the loop from regulating total active power, since it becomes unable to measure the error on this quantity. A matrix like the one used in (3.6) can be used to perform this operation. After these considerations, the controller structure becomes the one depicted in Fig. 3-2, where the matrix T represents the linear transformation removing homopolar components:

$$T \triangleq \begin{bmatrix} \frac{2}{3} & -\frac{1}{3} & -\frac{1}{3} \\ -\frac{1}{3} & \frac{2}{3} & -\frac{1}{3} \\ -\frac{1}{3} & -\frac{1}{3} & \frac{2}{3} \end{bmatrix} \tag{3.7}$$

3.2.2 Control of two of the three phases of the inverter

In this section, a way to control active and reactive power in two of the three phases of the inverter is proposed. In this specific case suppose the controlled phases are the phases a and b, thus the controller should regulate P_a, Q_a, P_b and Q_b. This does not mean that P_c and Q_c are unregulated and free to vary: once P_a, Q_a, P_b and Q_b are fixed, then P_c and Q_c are also set to a specific value, being the three-phase system a three-wires one. For the synchronization loop, it is possible to close it around the sum of the controlled active powers, namely $P_{3\phi} = P_a + P_b$. Then, the per-phase active power loop should consider only P_a and P_b. In the previous section, the problem of the separation between per-phase and total active-power control actions has been discussed, and the matrix T defined in 3.7 to remove the homopolar component in the per-phase loop. This problem can still arise here, and the solution can be as simple as in the previous case. Given two signals x and y, the homopolar component can be removed by this transformation:

$$\begin{bmatrix} x' \\ y' \end{bmatrix} = \begin{bmatrix} x - \frac{x+y}{2} \\ y - \frac{x+y}{2} \end{bmatrix} = \underbrace{\begin{bmatrix} \frac{1}{2} & -\frac{1}{2} \\ -\frac{1}{2} & \frac{1}{2} \end{bmatrix}}_{T_{2\times 2}} \cdot \begin{bmatrix} x \\ y \end{bmatrix}$$

Similarly to the configuration in Fig. 3-2, it is possible to apply the matrix $T_{2\times 2}$ to the per-phase active-power tracking error $P_x^{ref} - P_x$ to prevent this loop from regulating the total active power. The reactive power loop should take as input only Q_a and Q_b. In this configuration, only the references $\bar{V}_a$ and $\bar{V}_b$ are generated from the controller, so it is necessary to find a way to generate the reference signal $\bar{V}_c$. Since this is a three-wires system, it seems a good idea to generate $\bar{V}_c$ such that no homopolar component is present in the three references:

$$\bar{V}_a + \bar{V}_b + \bar{V}_c = 0 \quad \Longrightarrow \quad \bar{V}_c = -\bar{V}_a - \bar{V}_b$$

. The block scheme in Fig. 3-3 shows the resulting configuration, where $x = a, b$.

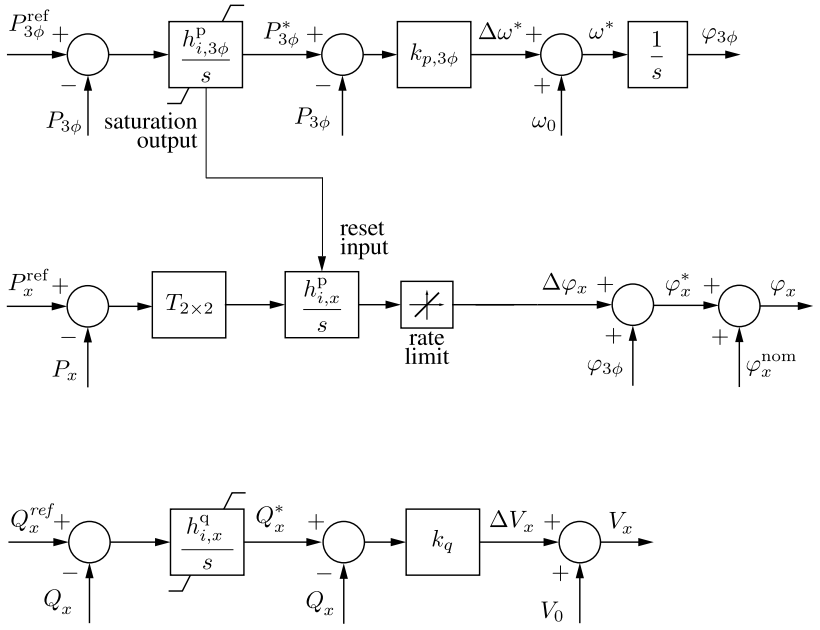

Figure 3-3: Control scheme where only two phases three phases of the inverter are regulated.

Chapter 4

Per-phase control analysis

An in-depth analysis of the closed-loop system is carried out in this chapter. State-space representation is derived and exploited to perform the design of the controller. State-in-mode participation factors are then computed, to achieve further insights into how the state variables contribute to the modal response of the system. Finally, a state-space representation is also derived for closed-loop three-phase four-wires systems, regulated by the controller proposed in [1].

4.1 State-space representation

In this section, the state-space representation of the system will be computed, in the form of:

$$\begin{cases} \dot{\boldsymbol{x}}(t) &= A\boldsymbol{x}(t) + B\boldsymbol{u}(t) \\ \boldsymbol{y}(t) &= C\boldsymbol{x}(t) + D\boldsymbol{u}(t) \end{cases}$$

where $\boldsymbol{x}(t)$ is the system state vector, $\boldsymbol{u}(t)$ is the vector of the input signals and $\boldsymbol{y}(t)$ is the vector of the output signals. The state-space representation is computed by assigning a state-variable to each integrator output, while power references are considered as the system input vector and measured inverter per-phase powers are

taken as the system output vector, obtaining the following definitions:

$$\boldsymbol{x} = \begin{bmatrix} \varphi_{3\phi} \\ \Delta\varphi_a \\ \Delta\varphi_b \\ \Delta\varphi_c \\ P^*_{3\phi} \\ Q^*_{3\phi} \end{bmatrix} \in \mathbb{R}^6, \quad \boldsymbol{u} = \begin{bmatrix} P_a^{ref} \\ P_b^{ref} \\ P_c^{ref} \\ Q_{3\phi}^{ref} \end{bmatrix} \in \mathbb{R}^4, \quad \boldsymbol{y} = \begin{bmatrix} P_a \\ P_b \\ P_c \\ Q_a \\ Q_b \\ Q_c \end{bmatrix} \in \mathbb{R}^6$$

The resulting state-space matrices are $A \in \mathbb{R}^{6\times6}$, $B \in \mathbb{R}^{6\times4}$, $C \in \mathbb{R}^{6\times6}$ and $D \in \mathbb{R}^{6\times4}$. By inspection of the block scheme in Fig. 3-2, it is possible derive the following expressions for the time derivatives of the state variables:

$$\begin{aligned}
\dot{\varphi}_{3\phi} &= k_{p,3\phi}\left[P^*_{3\phi} - (P_a + P_b + P_c)\right] \\
\dot{\Delta\varphi_a} &= h^{\mathrm{p}}_{i,a}\left[+\frac{2}{3}P_a^{ref} - \frac{1}{3}P_b^{ref} - \frac{1}{3}P_c^{ref} - \left(+\frac{2}{3}P_a - \frac{1}{3}P_b - \frac{1}{3}P_c\right)\right] \\
\dot{\Delta\varphi_b} &= h^{\mathrm{p}}_{i,b}\left[-\frac{1}{3}P_a^{ref} + \frac{2}{3}P_b^{ref} - \frac{1}{3}P_c^{ref} - \left(-\frac{1}{3}P_a + \frac{2}{3}P_b - \frac{1}{3}P_c\right)\right] \\
\dot{\Delta\varphi_c} &= h^{\mathrm{p}}_{i,c}\left[-\frac{1}{3}P_a^{ref} - \frac{1}{3}P_b^{ref} + \frac{2}{3}P_c^{ref} - \left(-\frac{1}{3}P_a - \frac{1}{3}P_b + \frac{2}{3}P_c\right)\right] \\
\dot{P}^*_{3\phi} &= h^{\mathrm{p}}_{i,3\phi}\left[\left(P_a^{ref} + P_b^{ref} + P_c^{ref}\right) - (P_a + P_b + P_c)\right] \\
\dot{Q}^*_{3\phi} &= h^{\mathrm{q}}_{i,3\phi}\left[Q_{3\phi}^{ref} - (Q_a + Q_b + Q_c)\right]
\end{aligned} \tag{4.1}$$

From Fig. 3-2 it is also possible to write $\Delta V = k_{q,3\phi}\left(Q^*_{3\phi} - Q_{3\phi}\right)$, and remembering that $Q_{3\phi} = \sum_x Q_x$ it is possible to combine these equations with the last three rows of the matrix equation in (2.18), obtaining

$$\Delta V = \frac{k_{q,3\phi}}{1 + 3k_{q,3\phi}\gamma_q} Q^*_{3\phi} \tag{4.2}$$

Then, by using this last one in (2.18) it is possible to obtain the expressions of the per-phase reactive power with respect to the state variables:

$$\begin{cases} Q_a = \frac{\sqrt{3}}{6}\gamma_p\left(\Delta\varphi_c - \Delta\varphi_b\right) + \frac{\gamma_q k_{q,3\phi}}{1+3\gamma_q k_{q,3\phi}} Q^*_{3\varphi} \\ Q_b = \frac{\sqrt{3}}{6}\gamma_p\left(\Delta\varphi_a - \Delta\varphi_c\right) + \frac{\gamma_q k_{q,3\phi}}{1+3\gamma_q k_{q,3\phi}} Q^*_{3\varphi} \\ Q_c = \frac{\sqrt{3}}{6}\gamma_p\left(\Delta\varphi_b - \Delta\varphi_a\right) + \frac{\gamma_q k_{q,3\phi}}{1+3\gamma_q k_{q,3\phi}} Q^*_{3\varphi} \end{cases} \tag{4.3}$$

The expressions of the per-phase active power can be obtained from (2.18):

$$\begin{cases} P_a = \gamma_p\varphi_{3\phi} + \frac{2}{3}\gamma_p\Delta\varphi_a + \frac{1}{6}\gamma_p\Delta\varphi_b + \frac{1}{6}\gamma_p\Delta\varphi_c = \gamma_p\varphi_{3\phi} + \frac{1}{2}\gamma_p\Delta\varphi_a \\ P_b = \gamma_p\varphi_{3\phi} + \frac{1}{6}\gamma_p\Delta\varphi_a + \frac{2}{3}\gamma_p\Delta\varphi_b + \frac{1}{6}\gamma_p\Delta\varphi_c = \gamma_p\varphi_{3\phi} + \frac{1}{2}\gamma_p\Delta\varphi_b \\ P_c = \gamma_p\varphi_{3\phi} + \frac{1}{6}\gamma_p\Delta\varphi_a + \frac{1}{6}\gamma_p\Delta\varphi_b + \frac{2}{3}\gamma_p\Delta\varphi_c = \gamma_p\varphi_{3\phi} + \frac{1}{2}\gamma_p\Delta\varphi_c \end{cases} \tag{4.4}$$

where the last equivalence is infered from the presence of the matrix T: indeed, summing the 2nd, 3rd and 4th equations in (4.1) one gets zero, thus the value of $\sum_x \Delta\varphi_x$ is equal to its initialization value, which can be assumed to be zero. The expressions of the matrices C and D are then directly derived from (4.3), (4.4):

$$C = \begin{bmatrix} \gamma_p & \frac{1}{2}\gamma_p & 0 & 0 & 0 & 0 \\ \gamma_p & 0 & \frac{1}{2}\gamma_p & 0 & 0 & 0 \\ \gamma_p & 0 & 0 & \frac{1}{2}\gamma_p & 0 & 0 \\ 0 & 0 & -\frac{\sqrt{3}}{6}\gamma_p & \frac{\sqrt{3}}{6}\gamma_p & 0 & \frac{\gamma_q k_{q,3\phi}}{1+3\gamma_q k_{q,3\phi}} \\ 0 & \frac{\sqrt{3}}{6}\gamma_p & 0 & -\frac{\sqrt{3}}{6}\gamma_p & 0 & \frac{\gamma_q k_{q,3\phi}}{1+3\gamma_q k_{q,3\phi}} \\ 0 & -\frac{\sqrt{3}}{6}\gamma_p & \frac{\sqrt{3}}{6}\gamma_p & 0 & 0 & \frac{\gamma_q k_{q,3\phi}}{1+3\gamma_q k_{q,3\phi}} \end{bmatrix}, \quad D = [0]_{6\times 4}$$

By substituting (4.3), (4.4) in (4.1) one can express the time derivative of the state variables as a linear combination of state variables themselves and system inputs,

allowing to find the expression of the matrices A and B:

$$A = \begin{bmatrix} -3\gamma_p k_{p,3\phi} & 0 & 0 & 0 & k_{p,3\phi} & 0 \\ 0 & -\frac{1}{2}h^{\mathrm{p}}_{i,a}\gamma_p & 0 & 0 & 0 & 0 \\ 0 & 0 & -\frac{1}{2}h^{\mathrm{p}}_{i,b}\gamma_p & 0 & 0 & 0 \\ 0 & 0 & 0 & -\frac{1}{2}h^{\mathrm{p}}_{i,c}\gamma_p & 0 & 0 \\ -3h^{\mathrm{p}}_{i,3\phi}\gamma_p & 0 & 0 & 0 & 0 & 0 \\ 0 & 0 & 0 & 0 & 0 & -h^{\mathrm{q}}_{i,3\phi}\frac{3\gamma_q k_{q,3\phi}}{1+3\gamma_q k_{q,3\phi}} \end{bmatrix}$$

$$B = \begin{bmatrix} 0 & 0 & 0 & 0 \\ \frac{2}{3}h^{\mathrm{p}}_{i,a} & -\frac{1}{3}h^{\mathrm{p}}_{i,b} & -\frac{1}{3}h^{\mathrm{p}}_{i,c} & 0 \\ -\frac{1}{3}h^{\mathrm{p}}_{i,a} & \frac{2}{3}h^{\mathrm{p}}_{i,b} & -\frac{1}{3}h^{\mathrm{p}}_{i,c} & 0 \\ -\frac{1}{3}h^{\mathrm{p}}_{i,a} & -\frac{1}{3}h^{\mathrm{p}}_{i,b} & \frac{2}{3}h^{\mathrm{p}}_{i,c} & 0 \\ h^{\mathrm{p}}_{i,3\phi} & h^{\mathrm{p}}_{i,3\phi} & h^{\mathrm{p}}_{i,3\phi} & 0 \\ 0 & 0 & 0 & h^{\mathrm{q}}_{i,3\phi} \end{bmatrix}$$

4.1.1 Controller design

As done in Section 3.1.1, the design of the controller should start from the design of the droop coefficients $k_{p,3\phi}$, $k_{q,3\phi}$ and the saturation values for the integrators. This can be done by following the same considerations carried out in Section 3.1.1. The saturation levels for the integrator in the synchronization loop can be found using the very same procedure leading to (3.4). For what concerns the reactive power loop, the Q-V droop law is slightly different since it is referring to total three-phase reactive power, not per-phase one. Thus equation (3.5) becomes the following:

$$Q^{*max,min}_{3\phi} = \pm S_N + \frac{V_{max,min} - V_0}{k_{q,3\phi}} \tag{4.5}$$

State-space representation is exploited to compute the gain of the integrators: it is possible to compute the location of the eigenvalues considering these gains as control variables and perform the design by allocating the eigenvalues of the system. Computing $\det(sI - A)$ it is possible to determine the characteristic polynomial of the

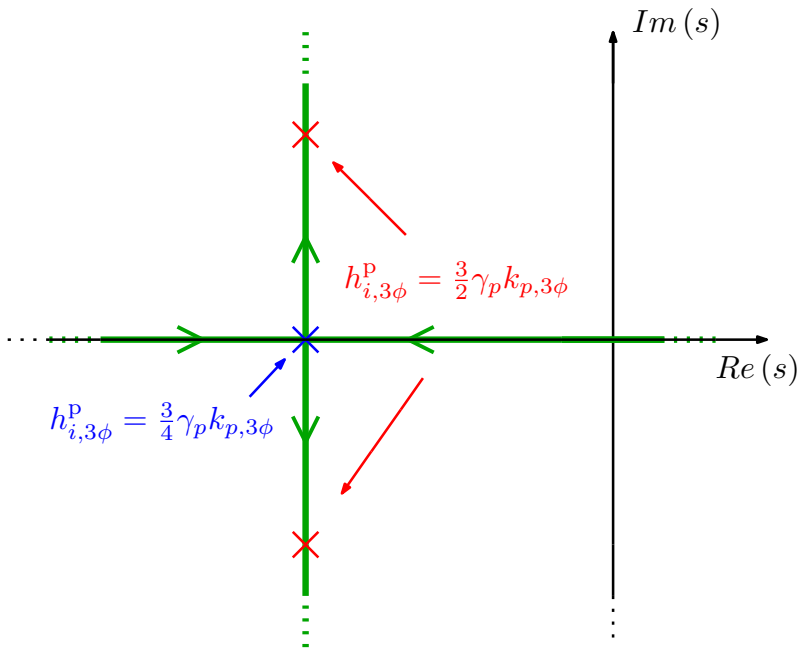

Figure 4-1: Eigenvalues relative to the synchronization loop.

system, whose roots are the system eigenvalues:

$$\psi(s) = \left(s + h^{\mathrm{q}}_{i,3\phi}\frac{3\gamma_q k_{q,3\phi}}{1+3\gamma_q k_{q,3\phi}}\right)\left(s+\frac{1}{2}\gamma_p h^{\mathrm{p}}_{i,a}\right)\left(s+\frac{1}{2}\gamma_p h^{\mathrm{p}}_{i,b}\right)\left(s+\frac{1}{2}\gamma_p h^{\mathrm{p}}_{i,c}\right)\cdot \\ \cdot\left(s^2+3\gamma_p k_{p,3\phi}s+3\gamma_p k_{p,3\phi}h^{\mathrm{p}}_{i,3\phi}\right) \tag{4.6}$$

By setting the values of $h^{\mathrm{q}}_{i,3\phi}$ and $h^{\mathrm{p}}_{i,x}$, $x = a,b,c$ it is possible to move the relative eigenvalues along the real axis. For what concerns the value of $h^{\mathrm{p}}_{i,3\phi}$, the relative eigenvalues are the solutions of

$$s^2+3\gamma_p k_{p,3\phi}s+3\gamma_p k_{p,3\phi}h^{\mathrm{p}}_{i,3\phi}=0$$

which leads to the following eigenvalue pair:

$$\lambda_{1,2} = \frac{-3\gamma_p k_{p,3\phi} \pm \sqrt{9\left(\gamma_p k_{p,3\phi}\right)^2 - 12h^{\mathrm{p}}_{i,3\phi}\gamma_p k_{p,3\phi}}}{2}$$

The eigenlocus of $\lambda_{1,2}$ is shown in Fig. 4-1. By setting $h^{\mathrm{p}}_{i,3\phi} = \frac{3}{4}\gamma_p k_{p,3\phi}$ one gets the critically damped solution, namely two coincedent real poles. By increasing the gain

value to $h^{\mathrm{p}}_{i,3\phi} = \frac{3}{2}\gamma_p k_{p,3\phi}$ it is possible to obtain a damping factor $\xi = \frac{1}{\sqrt{2}}$.

A possible design choice could be to set all the time constant to the same value. By choosing, for example, a damping factor $\xi = \frac{1}{\sqrt{2}}$, the target time constant becomes then $\sigma^* = \frac{3}{2}\gamma_p k_{p,3\phi}$. It is possible to impose this specific time constant to the other eigenvalues:

$$\begin{aligned} h^{\mathrm{q}}_{i,3\phi} &= \frac{1 + 3\gamma_q k_{q,3\phi}}{3\gamma_q k_{q,3\phi}}\sigma^* \\ h^{\mathrm{p}}_{i,x} &= \frac{2}{\gamma_p}\sigma^* \end{aligned} \tag{4.7}$$

4.2 Participation factors analysis

Participation factors were proposed in the early 80s [8] as a way to measure the relative contribution of a system mode to a state variable (mode-in-state participation factors) or to measure how state variables contributed to the modal response of the system (state-in-mode participation factors). In their original definition, state-in-mode and mode-in-state participation factors are identical, namely, the measure of participation for a state in a mode is the same as the participation for that mode in that state. However, dichotomies may arise using the original definition [5], so a different approach was proposed, which consists in averaging over an uncertain set of initial conditions. This latter approach has been found occasionally leading to ambiguities in participation factors when considering complex conjugate eigenvalues, bringing a slightly different definition [6]. In case of real eigenvalues, the definitions in [5] and [6] coincides.

To apply the method proposed in [6], a statistical description of initial conditions is needed. Power references P_a^{ref}, P_b^{ref}, P_c^{ref} and $Q_{3\phi}^{ref}$ have been modeled as independent uniformly distributed random variables. Then the needed statistical description of state-variables has been computed by expressing their steady-state value as combination of P_a^{ref}, P_b^{ref}, P_c^{ref} and $Q_{3\phi}^{ref}$. This approach comes with an inherent assumption: system reference changes are supposed to happen only when the system is in a steady state. This assumption may be appropriated if power references are

fed as output setpoints, while may not be appropriated if power references are fed as continuously time-varying control laws. The aforementioned statistical description of state-variables that is needed for this approach is the expected value of the product of each possible couple of state variables, namely

$$E\left[x_h x_k\right]; \quad h,k = 1,2,...,6$$

where x_h, x_k are the h-th and k-th component of the state vector x.

In order to compute the needed expected values, let us model the four power references, as previously said, as indipendendt random variables, uniformly distributed in $[-\alpha, \alpha]$, except for $Q_{3\phi}^{ref}$ which is supposed to be uniformly distributed in $[-3\alpha, 3\alpha]$. Also, in this computations we are considering frequency and voltage variations around their nominal values ω_0, V_g[1]. This means that in Fig. 3-2 the signals ω_0 and V_g are considered zero. Let us begin by computing the steady-state value of the state-variables with respect to P_a^{ref}, P_b^{ref}, P_c^{ref} and $Q_{3\phi}^{ref}$. In steady-state it is possible to assume $P_x = P_x^{ref}$ and $Q_{3\phi} = Q_{3\phi}^{ref}$. Then, it is possible to find an expression for $\varphi_{3\phi}$ and Δphi_x using (2.18):

$$\begin{bmatrix} \varphi_a \\ \varphi_b \\ \varphi_c \\ \Delta V \end{bmatrix} = \frac{1}{6} \begin{bmatrix} 4\gamma_p & \gamma_p & \gamma_p & 0 \\ \gamma_p & 4\gamma_p & \gamma_p & 0 \\ \gamma_p & \gamma_p & 4\gamma_p & 0 \\ 0 & 0 & 0 & 18\gamma_q \end{bmatrix}^{-1} \cdot \begin{bmatrix} P_a \\ P_b \\ P_c \\ Q_{3\varphi} \end{bmatrix}$$

where in this case $\varphi_x = \varphi_{3\phi} + \Delta\varphi_x$. This leads to:

$$\varphi_{3\phi} = \frac{P_a + P_b + P_c}{3\gamma_p}$$

$$\Delta\varphi_a = \frac{4}{3\gamma_p} P_a - \frac{2}{3\gamma_p} P_b - \frac{2}{3\gamma_p}$$

[1]Particularly for $\varphi_{3\phi}$ which is an instantaneous phase value, the objective here is to study how it contributes to power exchange, thus the important information is its displacement with respect to the instantaneous phase of the grid voltage.

$$\Delta\varphi_b = -\frac{2}{3\gamma_p}P_a + \frac{4}{3\gamma_p}P_b - \frac{2}{3\gamma_p}$$

$$\Delta\varphi_a = -\frac{2}{3\gamma_p}P_a - \frac{2}{3\gamma_p}P_b + \frac{4}{3\gamma_p}$$

Then, by inspection of Fig. 3-2 it is possible to write $P^*_{3\phi} = P_a + P_b + P_c$ since $\Delta\omega^* = 0$ in steady-state. Finally,

$$Q^*_{3\phi} = \left(1 + \frac{1}{3\gamma_q k_{q,3\phi}}\right)$$

which is the same equation used to find the saturation levels of the integrator in the reactive power loop. It is now possible to compute the expected values aforementioned:

$$E\left[\varphi^2_{3\phi}\right] = \left(\frac{1}{3\gamma_p}\right)^2 E\left[P_a^2 + P_b^2 + P_c^2\right] = \left(\frac{\alpha}{3\gamma_p}\right)^2$$

$$E\left[\varphi_{3\phi}\Delta\varphi_a\right] = \left(\frac{1}{3\gamma_p}\right)^2 E\left[4P_a^2 - 2P_b^2 - 2P_c^2\right] \overset{\text{i.i.d.}}{=} 0$$

$$\implies \quad E\left[\varphi_{3\phi}\Delta\varphi_x\right] = 0; \quad x = a, b, c$$

$$E\left[\varphi_{3\phi}P^*_{3\phi}\right] \overset{\text{i.i.d.}}{=} \frac{1}{3\gamma_p}E\left[P_a^2 + P_b^2 + P_c^2\right] = \frac{\alpha^2}{3\gamma_p}$$

$$E\left[\varphi_{3\phi}Q^*_{3\phi}\right] = \frac{1}{3\gamma_p}E\left[\left(P_a + P_b + P_c\right)Q^*_{3\phi}\right] \overset{\text{i.i.d.}}{=} 0$$

$$E\left[\Delta\varphi_a^2\right] = \left(\frac{1}{3\gamma_p}\right)^2 E\left[(4P_a - 2P_b - 2P_c)^2\right] = \frac{8\alpha^2}{9\gamma_p^2} = E\left[\Delta\varphi_b^2\right] = E\left[\Delta\varphi_a^2\right]$$

$$E\left[\Delta\varphi_a\Delta\varphi_b\right] = \left(\frac{1}{3\gamma_p}\right)^2 E\left[(4P_a - 2P_b - 2P_c)(-2P_a + 4P_b - 2P_c)\right] \overset{\text{i.i.d.}}{=}$$

$$\overset{\text{i.i.d.}}{=} \left(\frac{1}{3\gamma_p}\right)^2 E\left[-8P_a^2 - 8P_b^2 + 4P_c^2\right] = -4\left(\frac{\alpha}{3\gamma_p}\right)^2$$

$$\implies \quad E\left[\Delta\varphi_x\Delta\varphi_y\right] = -4\left(\frac{\alpha}{3\gamma_p}\right)^2; \quad x, y = a, b, c; \quad x \neq y$$

$$E\left[\Delta\varphi_a P^*_{3\phi}\right] = \frac{1}{3\gamma_p}E\left[(4P_a - 2P_b - 2P_c)(P_a + P_b + P_c)\right] \overset{\text{i.i.d.}}{=}$$

$$\overset{\text{i.i.d.}}{=} \frac{1}{3\gamma_p}E\left[4P_a^2 - 2P_b^2 - 2P_c^2\right] = 0 = E\left[\Delta\varphi_b P^*_{3\phi}\right] = E\left[\Delta\varphi_c P^*_{3\phi}\right]$$

$$E\left[\Delta\varphi_a Q^*_{3\phi}\right] = \frac{1}{3\gamma_p} E\left[\left(4P_a - 2P_b - 2P_c\right) Q^*_{3\phi}\right] \overset{\text{i.i.d.}}{=} 0 = E\left[\Delta\varphi_b Q^*_{3\phi}\right] = E\left[\Delta\varphi_c Q^*_{3\phi}\right]$$

$$E\left[P^{*2}_{3\phi}\right] = E\left[P_a^2 + P_b^2 + P_c^2\right] = \alpha^2$$

$$E\left[P^*_{3\phi} Q^*_{3\phi}\right] = E\left[\left(P_a + P_b + P_c\right) Q^*_{3\phi}\right] = 0$$

$$E\left[Q^{*2}_{3\phi}\right] = \left(1 + \frac{1}{3\gamma_q k_{3\phi}}\right)^2 E\left[Q^2_{3\phi}\right] = \left(1 + \frac{1}{3\gamma_q k_{3\phi}}\right)^2 3\alpha^2$$

In [6], the participation factor of the k-th state in the i-th mode is defined as:

$$\bar{\pi}_{ki} = \frac{E\left[\left(l^i_k x^0_k\right)^* z^0_i + z^{0*}_i \left(l^i_k x^0_k\right)\right]}{2E\left[z^{0*}_i z^0_i\right]} \tag{4.8}$$

where x^0_k is the k-th component of the state vector initial condition (random variable), l^i_k is the k-th component of the i-th left (row) eigenvector of the state matrix A and $z^0_i = \sum_k l^i_k x^0_k$ is the i-th component of the diagonalized state vector initial condition.

By applying the definition (4.8), with the parameters shown in Table I, one obtains the participation factors shown in Table I.

Modes	**State variables**					
	$\varphi_{3\varphi}$	$\Delta\varphi_a$	$\Delta\varphi_b$	$\Delta\varphi_c$	$P^*_{3\varphi}$	$Q^*_{3\varphi}$
e^{λ_1}	0.00	0.00	0.00	0.00	**1.00**	0.00
e^{λ_2}	0.00	0.00	0.00	0.00	**1.00**	0.00
e^{λ_3}	0.00	**1.00**	0.00	0.00	0.00	0.00
e^{λ_4}	0.00	0.00	**1.00**	0.00	0.00	0.00
e^{λ_5}	0.00	0.00	0.00	**1.00**	0.00	0.00
e^{λ_6}	0.00	0.00	0.00	0.00	0.00	**1.00**

Table I: State-in-modes participation factors for modal analysis of the control.

4.3 Four-wires state-space representation

To conclude this chapter, a state-space representation for three-phase four-wires systems controlled by the regulator proposed in [1] is shown. To derive this representation, the gray-colored proportional path in Fig. 3-1 has been neglected. This makes the computation of the state-space representation much easier and allows to derive an easy procedure to design the controller through the allocation of the eigenvalues of

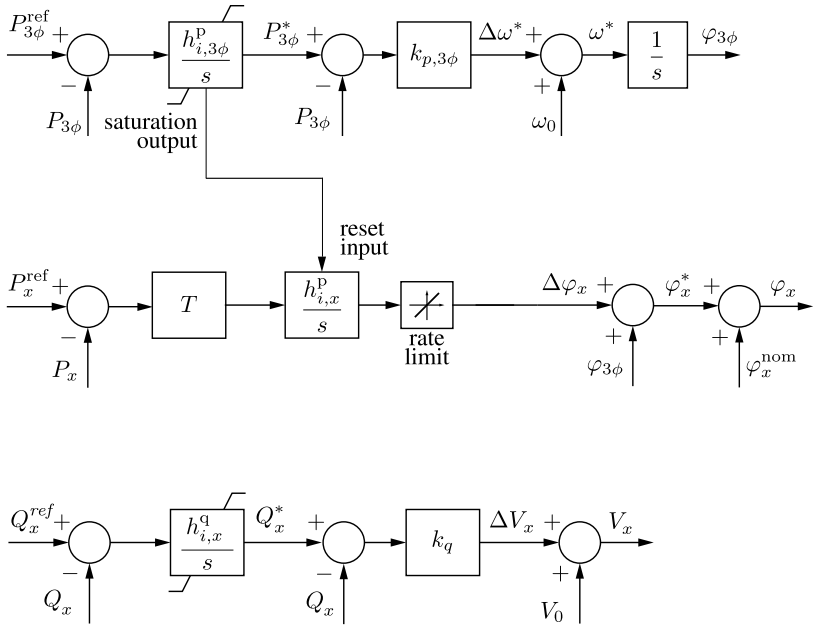

Figure 4-2: Three-phase four-wires systems controller considered for the state-space representation.

the system. Moreover, the process transfer function to be compensated in that loop can be assumed to simply be a proportional gain, thus 90° phase margin is guaranteed. This latter assumption is valid if the loop bandwidth is kept much below the bandwidth of the power measurement system. Another modification with respect the scheme in Fig. 3-1 is the presence of the pre-transformation matrix T, defined and discussed in Section 3.2.1. The scheme considered in this case becomes the one in Fig. 4-2.

Let us consider the same procedure carried out for the three-wires system: assign a state variable to the output of each integrator, consider the power references as system inputs and the measured power values as system outputs. System state, input

and output vectors are then:

$$x = \begin{bmatrix} \varphi_{3\phi} \\ \Delta\varphi_a \\ \Delta\varphi_b \\ \Delta\varphi_c \\ P^*_{3\phi} \\ Q^*_a \\ Q^*_b \\ Q^*_c \end{bmatrix}; \quad u = \begin{bmatrix} P^{ref}_a \\ P^{ref}_b \\ P^{ref}_c \\ Q^{ref}_a \\ Q^{ref}_b \\ Q^{ref}_c \end{bmatrix}; \quad y = \begin{bmatrix} P_a \\ P_b \\ P_c \\ Q_a \\ Q_b \\ Q_c \end{bmatrix} \tag{4.9}$$

This leads to the following state-space representation:

$$\begin{cases} \dot{x} &= Ax + Bu \\ y &= Cx + Du \end{cases}$$

where

$$A = \begin{bmatrix} -3\gamma_p k_{p,3\phi} & 0 & 0 & 0 & k_{p,3\phi} & 0 & 0 & 0 \\ 0 & -h^{\mathrm{p}}_{i,a} & 0 & 0 & 0 & 0 & 0 & 0 \\ 0 & 0 & -h^{\mathrm{p}}_{i,b} & 0 & 0 & 0 & 0 & 0 \\ 0 & 0 & 0 & -h^{\mathrm{p}}_{i,c} & 0 & 0 & 0 & 0 \\ -3h^{\mathrm{p}}_{i,3\phi}\gamma_p & 0 & 0 & 0 & 0 & 0 & 0 & 0 \\ 0 & 0 & 0 & 0 & 0 & -h^{\mathrm{q}}_{i,a}\frac{\gamma_q k_q}{1+\gamma_q k_q} & 0 & 0 \\ 0 & 0 & 0 & 0 & 0 & 0 & -h^{\mathrm{q}}_{i,b}\frac{\gamma_q k_q}{1+\gamma_q k_q} & 0 \\ 0 & 0 & 0 & 0 & 0 & 0 & 0 & -h^{\mathrm{q}}_{i,c}\frac{\gamma_q k_q}{1+\gamma_q k_q} \end{bmatrix}$$

$$B = \begin{bmatrix} 0 & 0 & 0 & 0 & 0 & 0 \\ \frac{2}{3}h^{\mathrm{p}}_{i,a} & -\frac{1}{3}h^{\mathrm{p}}_{i,b} & -\frac{1}{3}h^{\mathrm{p}}_{i,c} & 0 & 0 & 0 \\ -\frac{1}{3}h^{\mathrm{p}}_{i,a} & \frac{2}{3}h^{\mathrm{p}}_{i,b} & -\frac{1}{3}h^{\mathrm{p}}_{i,c} & 0 & 0 & 0 \\ -\frac{1}{3}h^{\mathrm{p}}_{i,a} & -\frac{1}{3}h^{\mathrm{p}}_{i,b} & \frac{2}{3}h^{\mathrm{p}}_{i,c} & 0 & 0 & 0 \\ h^{\mathrm{p}}_{i,3\phi} & h^{\mathrm{p}}_{i,3\phi} & h^{\mathrm{p}}_{i,3\phi} & 0 & 0 & 0 \\ 0 & 0 & 0 & h^{\mathrm{q}}_{i,a} & 0 & 0 \\ 0 & 0 & 0 & 0 & h^{\mathrm{q}}_{i,b} & 0 \\ 0 & 0 & 0 & 0 & 0 & h^{\mathrm{q}}_{i,c} \end{bmatrix}$$

$$C = \begin{bmatrix} \gamma_p & \gamma_p & 0 & 0 & 0 & 0 & 0 & 0 \\ \gamma_p & 0 & \gamma_p & 0 & 0 & 0 & 0 & 0 \\ \gamma_p & 0 & 0 & \gamma_p & 0 & 0 & 0 & 0 \\ 0 & 0 & 0 & 0 & 0 & \frac{\gamma_q k_q}{1+\gamma_q k_q} & 0 & 0 \\ 0 & 0 & 0 & 0 & 0 & 0 & \frac{\gamma_q k_q}{1+\gamma_q k_q} & 0 \\ 0 & 0 & 0 & 0 & 0 & 0 & 0 & \frac{\gamma_q k_q}{1+\gamma_q k_q} \end{bmatrix}; \quad D = [0]_{6\times 6}$$

By computing $\det(sI - A)$ one gets:

$$\psi(s) = \left(s + h^{\mathrm{q}}_{i,a}\frac{\gamma_q k_q}{1+\gamma_q k_q}\right)\left(s + h^{\mathrm{q}}_{i,b}\frac{\gamma_q k_q}{1+\gamma_q k_q}\right)\left(s + h^{\mathrm{q}}_{i,c}\frac{\gamma_q k_q}{1+\gamma_q k_q}\right)\cdot$$
$$\cdot\left(s+\gamma_p h^{\mathrm{p}}_{i,a}\right)\left(s+\gamma_p h^{\mathrm{p}}_{i,b}\right)\left(s+\gamma_p h^{\mathrm{p}}_{i,c}\right)\left(s^2 + 3\gamma_p k_{p,3\phi}s + 3\gamma_p k_{p,3\phi}h^{\mathrm{p}}_{i,3\phi}\right)$$

The controller gains can be set by keeping into account the same considerations carried out for (4.6).

Chapter 5

Results

Simulation and experimental results are collected, shown, and discussed here. Simulation results shows the operation of both the control schemes in Fig. 3-2 and in Fig. 3-3, while only scheme in Fig. 3-2 is considered during experimental tests.

5.1 Simulation results

The following simulation results are obtained by implementing an ideal switching model of the inverters connected to the grid. Inverters are controlled by a two-level control scheme:

- a zero-level controller, which is composed of an inner current loop, regulating the average output inductor current, and an outer voltage loop, regulating the output capacitor voltage;
- a primary-level controller, consisting of the per-phase power controller studied in this thesis, taking power references and generating output voltage reference for the zero-level controller.

Simulation results show that the per-phase power analysis done in Section 2.2 is correct. In particular, the control capabilities theoretically derived by the analysis in that section are verified by the simulations, in both the following control modes:

Parameter		Value	
P-f droop coefficient	$k_{p,3\phi}$	0.209	mHz/W
3-phase P saturation limit	$\pm P_{3\varphi}^{*\mathrm{sat}}$	± 6	kW
$Q-V$ droop coefficient	$k_{q,3\phi}$	1.8	mV/VAr
3-phase P control integral gain	$h_{i,3\varphi}^{\mathrm{p}}$	6.33	1/s
per-phase P control integral gain	$h_{i,x}^{\mathrm{p}}$	0.628	mrad/Ws
3-phase Q control integral gain	$h_{i,3\varphi}^{\mathrm{q}}$	12.6	1/s
nominal voltage amplitude	V_g	$110\sqrt{2}$	V
nominal frequency	ω	$2\pi\,(50)$	rad/s
inductive coupling impedance	L	1.9	mH

Table I: Control parameters used in simulation tests.

- Control of per-phase active power in all three phases and control of total reactive power;
- Control of active and reactive power in two out of three phases (P_a, P_b, Q_a, Q_b).

The transition towards the island condition is shown to be smooth and seamless from the load point of view. The control parameters used in simulation tests are shown in I.

5.1.1 Control of per-phase active power and total reactive power

The control scheme employed here is the one shown in Fig. 3-2, allowing control of per-phase active power and control of only total reactive power.

Grid-tied operation

This first test is a simple demonstration of the control capabilities. A 3 kW nominal power inverter is connected to a three-phase voltage grid, while power references are varied according to Table II.

The waveforms of the per-phase output power of the inverter are shown in Fig. 5-1. It is possible to notice that reactive power is also equally shared among the three phases under the balanced active-power load condition. Once the active-power load becomes unbalanced, reactive power among the three phases also gets unbalanced (as

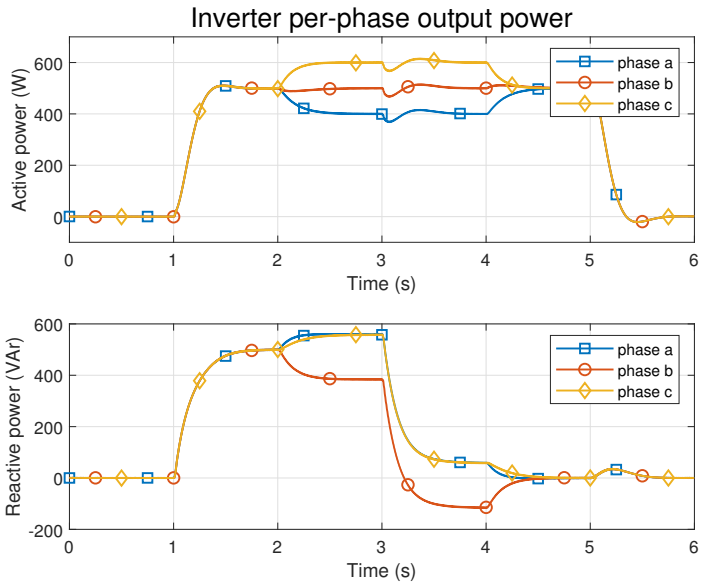

Figure 5-1: Power control during grid tied operation.

P_a^{ref}	0	500	600	600	500	0
P_b^{ref}	0	500	500	500	500	0
P_c^{ref}	0	500	400	400	500	0
$Q_{3\phi}^{ref}$	0	1500	1500	0	0	0
	$0 < t < 1$	$1 < t < 2$	$2 < t < 3$	$3 < t < 4$	$4 < t < 5$	$5 < t < 6$

Table II: Power reference signals with respect to time, during grid-tied simulation, while controlling P_a, P_b, P_c, $Q_{3\phi}$.

noticeable at $t = 2$ s). For each of the three phases, the reactive-power deviation from balanced sharing (namely $Q_{3\phi}^{ref}/3$) is independent of total reactive-power load, as can be seen at $t = 3$ s and $t = 4$ s.

Transition towards island operation

A way to regulate active-power during grid-tied operation is to change the reference value P^* in the droop characteristic

$$\omega = \omega_0 + k_p \left(P^* - P\right)$$

As long as ω_0 is the actual grid frequency, the regulation happens with zero error. However, grid frequency is not steady in practice, as it varies around its nominal value. Grid frequency deviations thus lead to unprecise, if not incorrect, power tracking. A possible approach would be to use a time-varying P-f droop law, where the frequency reference ω_0 is instead the actual grid frequency, obtained through a phase-locked loop for example. During grid-tied operation this would allow perfect power tracking, with zero error. However, when the grid is disconnected the grid frequency is no more externally imposed but depends on the operation of the inverters. This would cause the frequency to drift toward extremely high or low values, leading to the collapse of the entire microgrid. An example is shown in Fig. 5-2: a resistive load is connected to the grid together with two inverters, which are regulated to a varying P-f droop law as described before. At $t = 1$ s the grid is disconnected, and the frequency of the islanded microgrid starts drifting towards low values, leading to the collapse of the entire system.

The key feature of the controller analyzed in this thesis is the possibility to achieve a smooth transition toward island operation. The reference frequency in the P-f droop law implementation is kept fixed to the grid-frequency nominal value, and during grid-tied operation the power tracking error is forced to zero by varying P^* to account for grid frequency variations. This way when the grid is disconnected and the P^* value is saturated, the droop law becomes a fixed one: this way the grid frequency

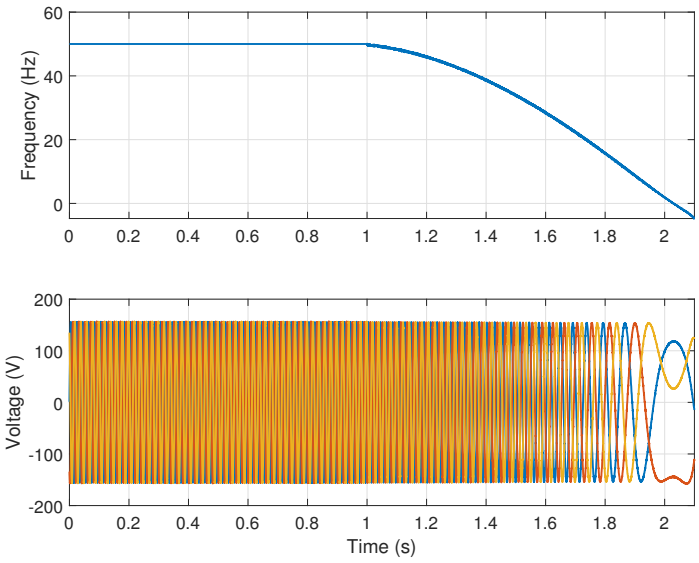

Figure 5-2: Microgrid frequency drifting away after disconnection with the main grid.

is correctly scaled based on the droop law and the transition is seamless from the load point of view, as shown in the following tests.

To perform the first test, two identical inverters (both in hardware and control parameters) are connected to the grid, together with a resistive balanced three-phase load and a grid-feeding converter. This latter converter is implemented, through an averaged model, as a variable three-phase current source, regulated to track active and reactive power reference signals. Two simulations have been done in this scenario, with different power reference signals for the inverters. The reactive power reference is always set to zero. Grid-feeding converter outputs 1.5 kW into the microgrid, while resistive load is a 10 Ω one, nominally absorbing $3 \cdot \frac{110^2}{10} = 3 \cdot (1210 \text{ kW})$ active power.

During the first simulation, both inverters are correctly tracking the same 2.4 kW active power reference signal in grid-tied operation. At $t = 1$ s the grid is disconnected: without the grid, power control is no more possible, since output power is imposed by the load. Also, the grid-feeding converter contributes to determining the whole power load of the microgrid seen by the two droop-operating inverters. Being the inverters two identical ones initially supplying the same power, their droop laws should be the same the instant right after grid disconnection, leading them to equally share the

power load. The microgrid active-power load can be approximated as:

$$P_{load} \simeq P_R - P_C \simeq 3\frac{110^2}{10} - 1.5 \text{ kW} \simeq 2.1 \text{ kW}$$

where P_R is the power dissipated by the resistive load and P_C is the power injected in the microgrid by the grid-feeding inverter. This means the two inverters should be supplying approximately 1 kW each, and the integrator in their synchronization loops should saturate towards its upper limit (being the total active-power error positive), obtaining finally the following fixed droop characteristic:

$$\omega = \omega_0 + k_{p,3\phi}\left(P^*_{3\phi,max} - P_{3\phi}\right)$$

The output power waveforms are shown in Fig. 5-3, and it is possible to notice that, as expected, the two inverters equally share the same power load, even during transient condition. In Fig. 5-4 is shown the microgrid voltage waveform in a small time interval including the grid disconnection instant. The smoothness of the transition can be inferred from the quality of the sinusoidal waveforms: from the load point of view, the transition is practically seamless.

For what concerns the second simulation, the microgrid structure is the same: two identical droop-controlled inverters, the same resistive load as the previous simulation, and also the same grid-feeding converter. The inverters, however, now are tracking two different active power reference signals: the first one is absorbing the 1.5 kW active power injected by the grid-feeding converter, while the other one is supplying the grid with 2.4 kW. Output power waveforms are shown in Fig. 5-5. When grid disconnection happens, because of the different reference signals the two integrators in the synchronization loops start saturating in opposite directions. Because of the initially different droop-characteristic, the power load is not equally shared, causing the second inverter to reach the islanding condition first. When it starts operating with a fixed droop characteristic, the first inverter becomes able to regulate output power: this happens around $t \simeq 3.35$ s. From this time instant, the first inverter starts regulating its output power to track the -1.5 kW reference signal, while the second

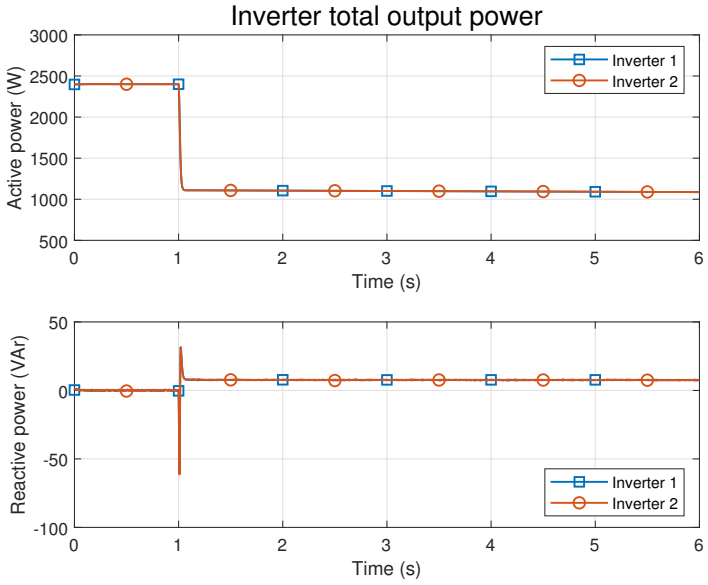

Figure 5-3: Inverters output power waveforms during transition towards island operation.

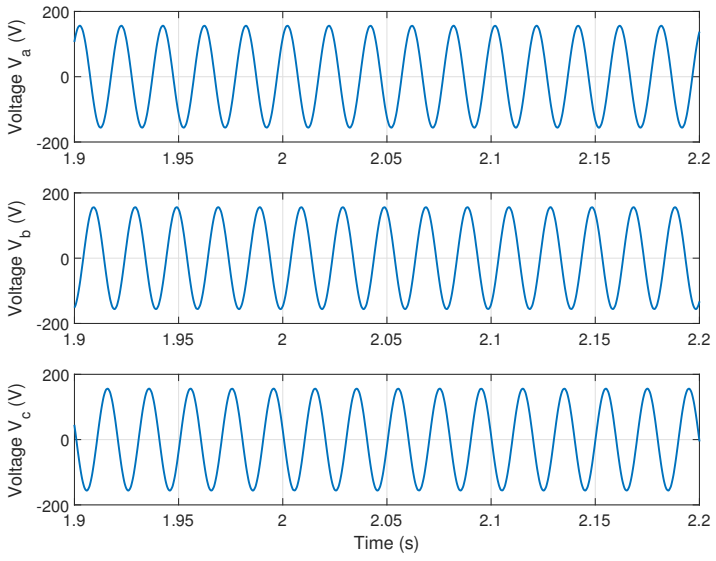

Figure 5-4: Microgrid voltage waveforms during island transition.

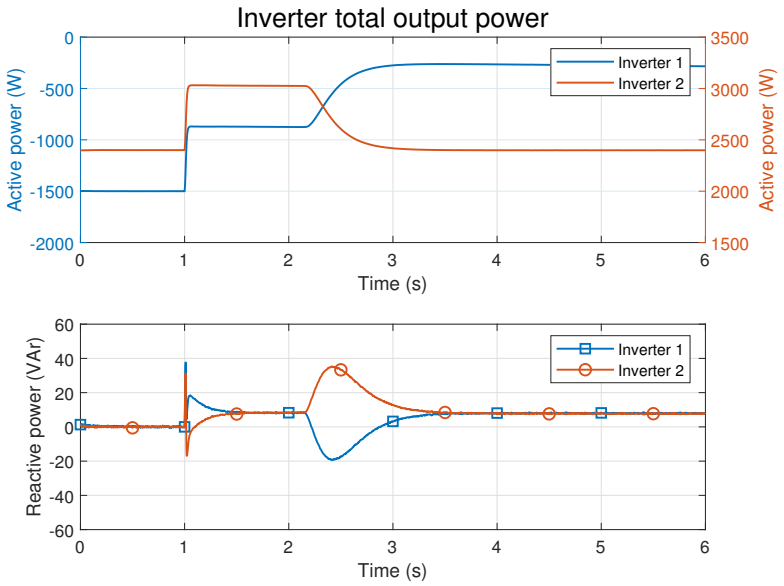

Figure 5-5: Output power waveforms for the two inverters during island transition.

inverter substitutes the grid in the microgrid, supplying the resistive load. Similarly to Fig. 5-4, in Fig. 5-6 it is possible to look at the microgrid voltage waveforms, to confirm the smoothness of the transition towards island condition.

To correctly interpret the results obtained by these two latter simulations, it is important to keep in mind the objective of the controller: the first one is to be able to regulate per-phase active power and total reactive power during grid-tied operation, and the second one is to be able to bring the microgrid towards the operation in island condition in a way that should be as smooth as possible, and possibly seamless for the loads connected to the microgrid.

The first simulation shows that active-power load (and reactive one too) is equally shared between the two inverters. While this can be a good strategy during the transition, there can be better strategies to manage the power load sharing than basing the proportions on nominal power. One could, for example, consider the energy storage system supplying the inverter and take into account its charge level. Other strategies could try to minimize the power lost. The second simulation shows that the first inverter does not recognize the islanding condition. This, also, is not a favorable situation to operate in but could be tolerated during the transition.

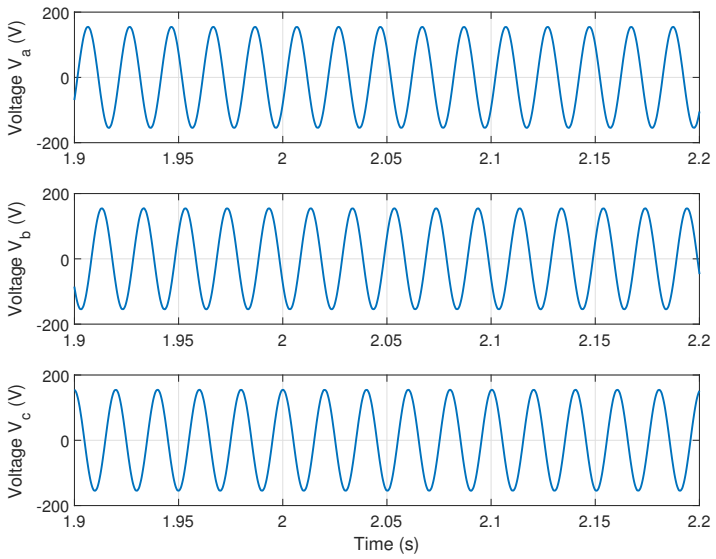

Figure 5-6: Microgrid voltage waveforms during island transition.

All these arguments are to point out the fact that the grid could not be optimally managed right after the transition because the goal is to make it happen as smoothly as possible. Adjustments can however be made after the transition is concluded: droop characteristic references and/or coefficients could be changed, and inverters still not operating in islanding conditions could be brought to that operating condition.

Supply of unbalanced loads

This last simulation considers what could happen when a heavily unbalanced load is connected to the grid, and how this inverter could be supplying it to minimize the unbalance of the main grid.

The microgrid considered in this simulation is composed of one droop-controlled inverter, one unbalanced load, and the main grid, which is connected to the microgrid through a small resistive impedance (100 mΩ). The idea here is that the impedance sensed by the load towards the main grid should be higher than the one sensed towards the inverter (which is considered to be zero here) that is connected locally. Then, because of that impedance, if the unbalanced load is supplied by the main grid other devices in the microgrid would operate with an unbalanced voltage.

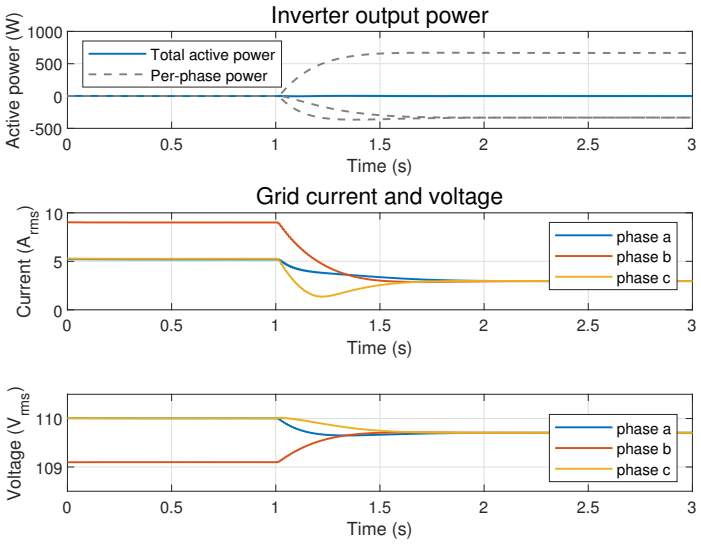

Figure 5-7: Inverter output power and grid voltage and current measurement during the balancing operation.

A possible solution is to supply the unbalanced power component of the load with the locally connected inverter, exploiting its per-phase power control capabilities. This operation can be done by keeping equal to zero the total active power supplied by the inverter, as shown in Fig. 5-7. Initially, the grid is supplying the unbalanced load, but because of its series impedance, the line voltage gets unbalanced too. At $t = 1$ s the inverter, by keeping its supplied total active power equal to zero, provides the unbalanced current component to the load. Being its output impedance, supposedly, lower than the grid one, the grid voltage now becomes balanced, since the grid is now injecting balanced currents.

5.1.2 Control of active and reactive power in two of the three inverter phases

The following tests demonstrate the possibility of controlling both active and reactive power in two phases of the system, in this case P_a, P_b, Q_a, Q_b. As previously discussed, P_c and Q_c are not unregulated and free to vary: they both depend on active and reactive power in the other two phases.

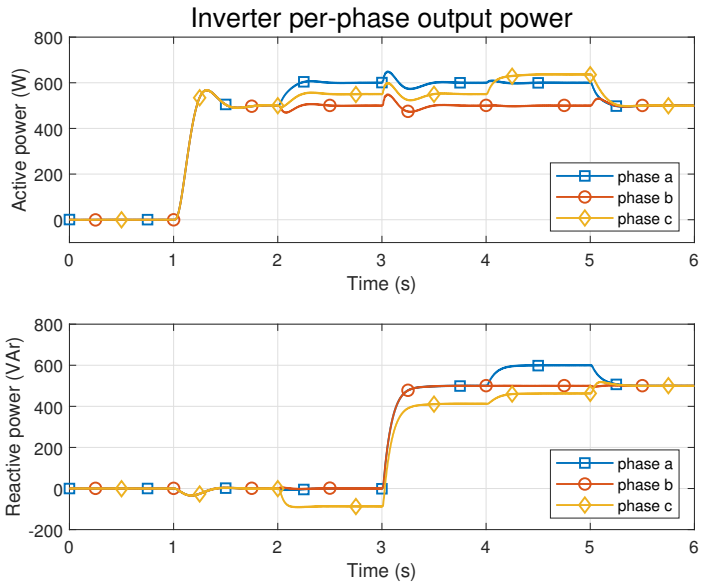

Figure 5-8: Output power waveforms during grid-tied operation, while controlling P_a, P_b, Q_a, Q_b.

P_a^{ref}	0	500	600	600	600	500
P_b^{ref}	0	500	500	500	500	500
Q_a^{ref}	0	0	0	500	600	500
Q_b^{ref}	0	0	0	500	500	500
	$0 < t < 1$	$1 < t < 2$	$2 < t < 3$	$3 < t < 4$	$4 < t < 5$	$5 < t < 6$

Table III: Power reference signals with respect to time, during grid-tied simulation, while controlling P_a, P_b, Q_a, Q_b.

Grid-tied operation

As done for the previous control mode, this first test setup is a single 3 kW nominal power three-phase inverter, connected to the main grid. Power reference signals are varied according to Table III.

From output power waveforms shown in Fig. 5-8, it is possible to see that P_c and Q_c are sensible to power unbalancement, both in active and reactive power. In any situation, however, P_a, P_b, Q_a, Q_b are correctly regulated.

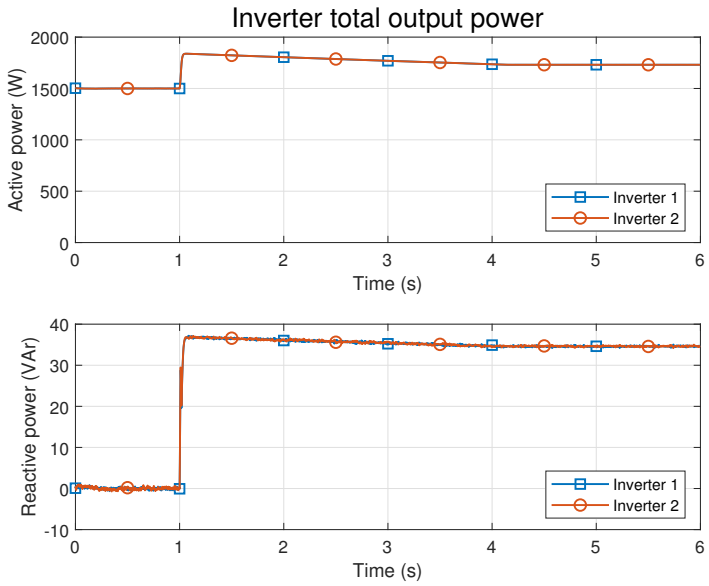

Figure 5-9: Output power waveforms during transition towards island operation, while controlling P_a, P_b, Q_a, Q_b.

Transition towards island operation

The following test shows that even in this control mode the transition towards island operation is smooth and seamless from the load point of view. Two 3 kW nominal power three-phase inverters are initially connected to the grid, together with a balanced 10 Ω three-phase load. During grid-tied operation, the inverters are both supplying the grid with 1.5 kW active power. At $t = 1$ s the grid is disconnected and the inverters equally supply the power absorbed by the load, as shown in Fig. 5-9.

In Fig. 5-10 it is possible to see that the transition is smooth, and no distortion is visible from the voltage waveforms during the disconnection of the main grid.

5.2 Experimental results

The following experimental results have been derived using the experimental prototype depicted in Fig. 5-11. Eight Imperix PEB8032 half-bridge modules were used to implement the converters. The control scheme in Fig. 3-2 was implemented on an Imperix B-Box RCP embedding a Xilinx Zynq 7030 SoC. Control tasks were executed

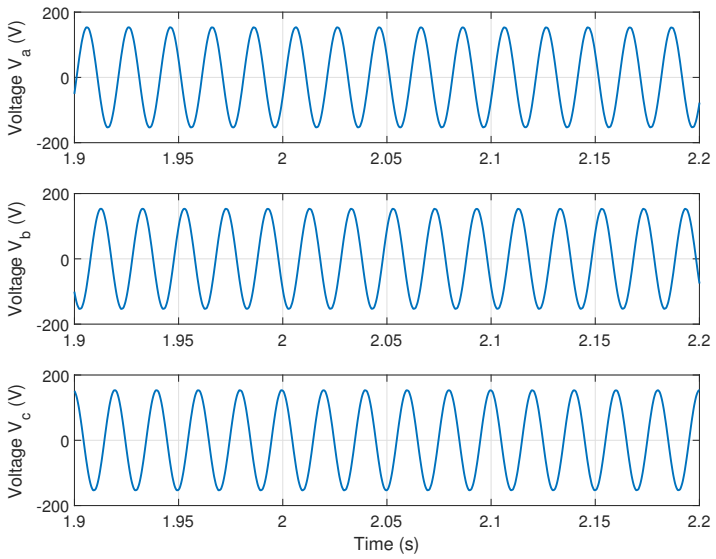

Figure 5-10: Microgrid voltage waveforms during grid disconnection.

twice per switching period, to perform a double-rate updated pulse-width modulation. The hardware specifications are shown in table Table IV, while control parameters are shown in Table V.

Step variation of active and reactive power

In these tests, a converter is connected to the grid, which is implemented using the remaining half-bridge modules in the prototype. Step-variations in active and reactive power reference signals are performed.

In Fig. 5-12 are shown the power waveforms (a) and voltage and current waveforms (b) of an active power step variation, from 0 to 1 kW for each phase simultaneously. It is possible to notice that active power in each phase is correctly following the reference signals, as total reactive power does. While the phase difference between each of the phase voltages is practically negligible, it is possible to see that, through frequency variations, the controller is providing the correct overall instantaneous phase shift. From current waveforms, it is possible to see the increase in delivered power.

In Fig. 5-13 a step variation of active power in phase C is considered, from 0 to 1 kW. From power waveforms in (a), it is possible to see that the system correctly

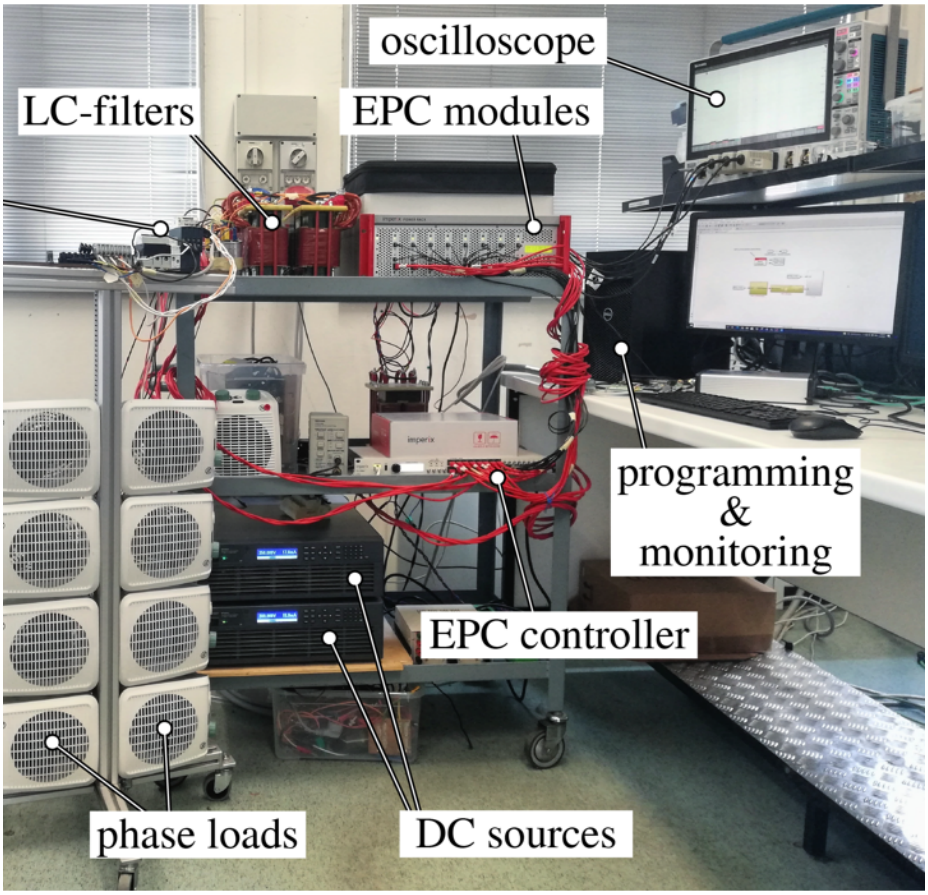

Figure 5-11: Experimental setup employed to perform the experimental tests.

Parameter		**Value**	
DC-link voltage	V_{dc}	350	V
DC-link capacitor	C_{dc}	3.3	mF
DC-link inductor	L_{dc}	2.5	mH
Output filter capacitor	C_f	50	μF
Output filter inductor	L_f	1.5	mH
Switching frequency	f_{sw}	20	kHz
Nominal power rating	S_N	3	kVA
Nominal grid voltage rms	V_g	110	V
Nominal grid frequency	ω_g	$2\pi\,(50)$	rad/s

Table IV: Hardware parameters of the experimental prototype.

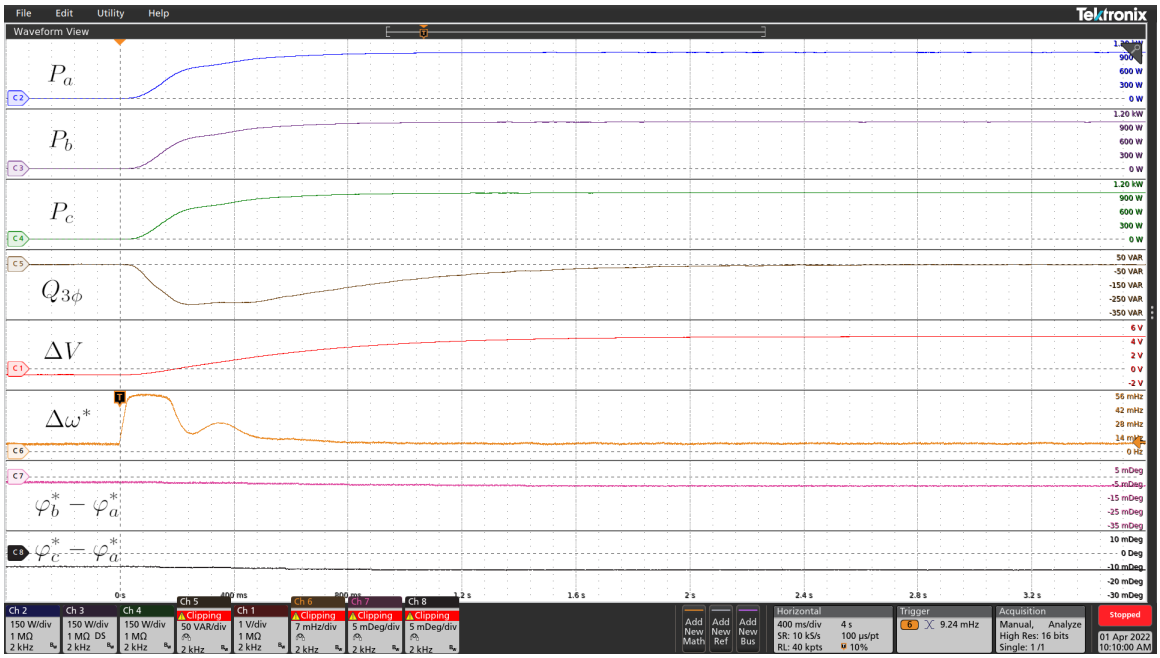

(a)

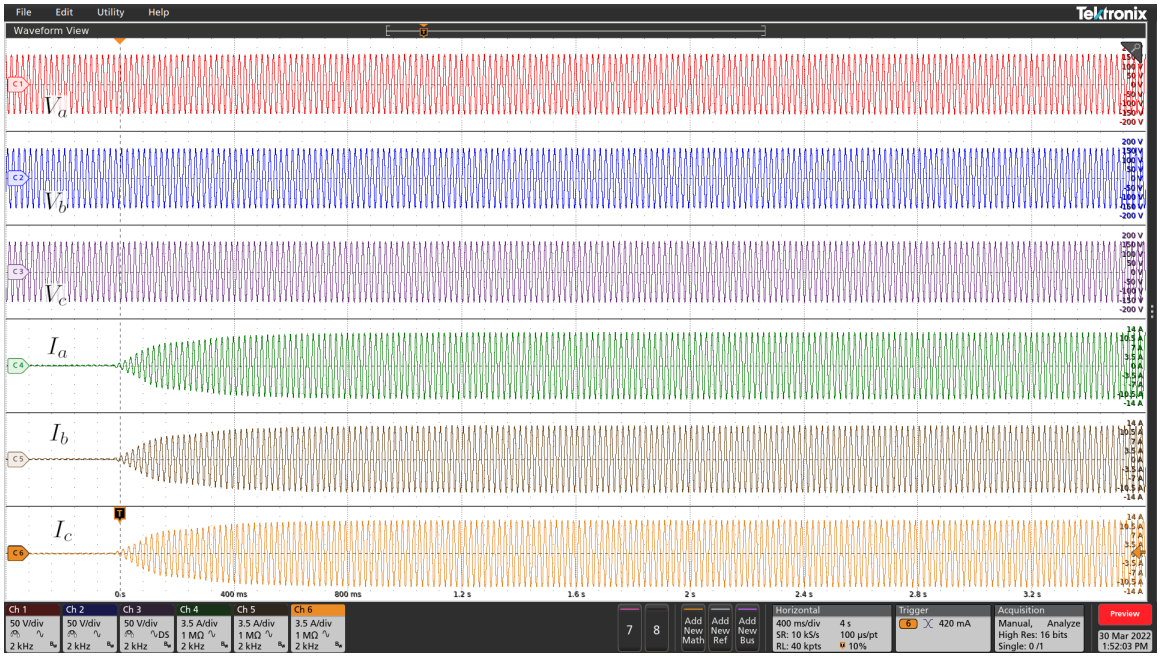

(b)

Figure 5-12: Grid tied inverter performing an active power step variation. At $t = 0$ s the reference step changes $P^{\text{ref}}_{a,b,c} : 0 \rightarrow 1$ kW.

Parameter		Value	
P-f droop coefficient	$k_{p,3\phi}$	0.209	mHz/W
Q-V droop coefficient	$k_{q,3\phi}$	0.917	mV/VAr
3-phase P saturation limit	$\pm P_{3\varphi}^{*\text{sat}}$	± 6	kW
3-phase Q saturation limit	$\pm Q_{3\varphi}^{*\text{sat}}$	± 6	kVAr
3-phase P control integral gain	$h_{i,3\varphi}^{\text{p}}$	3.6944	1/s
per-phase P control integral gain	$h_{i,x}^{\text{p}}$	0.62832	mrad/Ws
3-phase Q control integral gain	$h_{i,3\varphi}^{\text{q}}$	16.2608	1/s
nominal voltage amplitude	V_g	$110\sqrt{2}$	V
nominal frequency	ω	$2\pi\,(50)$	rad/s
inductive coupling impedance	L	3.3	mH

Table V: Control parameters used in experimental tests.

follows the reference signals. Through frequency variation, the overall phase shift is set based on total active power, while angle differences between phase voltages are set by the per-phase active power regulation loop. Current waveforms in (b) show that reactive power must be flowing in phases A and B even if total reactive power is regulated to zero, being their active power equal to zero.

Waveforms in Fig. 5-14 are the results of a step variation in active power for all three phases, from 0 to 1 kW. Then, at $t = 3$ s active power in phase C is set to zero. As in the other tests, power references are being correctly followed. Angle differences in phase voltages are negligible as long as balanced power is being supplied, as visible in the transition before and after $t = 3$ s.

Last step variation test, in Fig. 5-15, considers a total reactive power step variation, from 0 to 800 VAr. Reactive power reference is correctly tracked. An interesting thing to be noticed is the very low sensibility of active power to reactive power step variations. On the contrary, reactive power is much more sensible to active power variations, as can be seen in Fig. 5-12. The reason can be the fact that a change in the voltage amplitude does not affect the phase shift. However, a change in the phase shift modifies the delivered current, changing the voltage drop across potential resistive impedances.

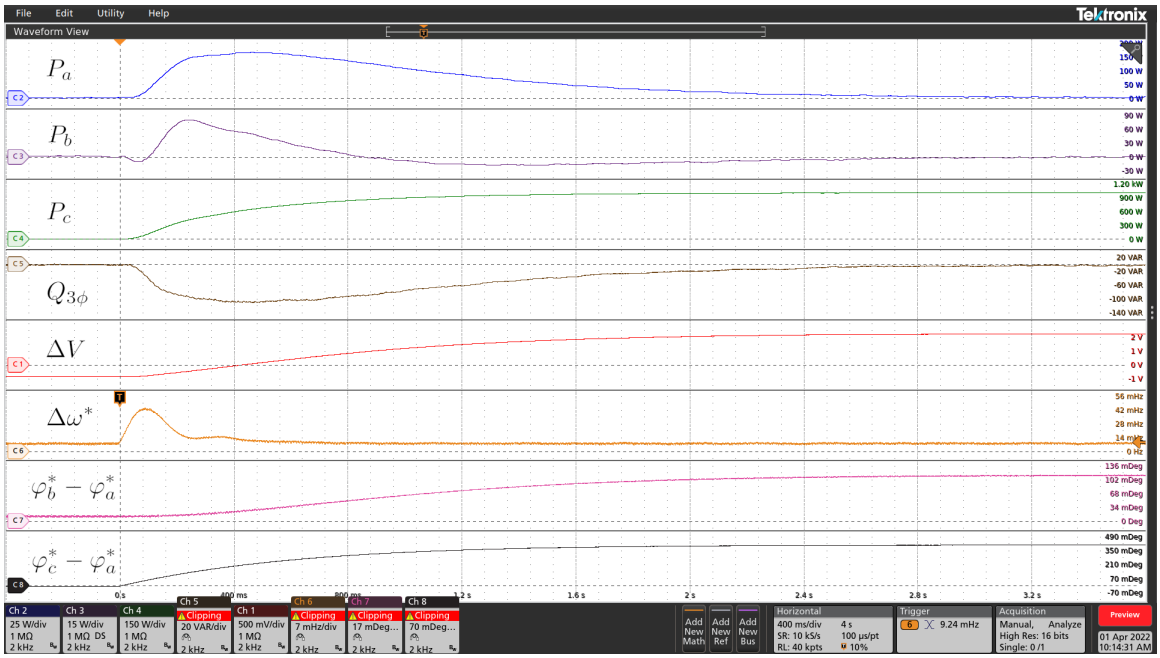

(a)

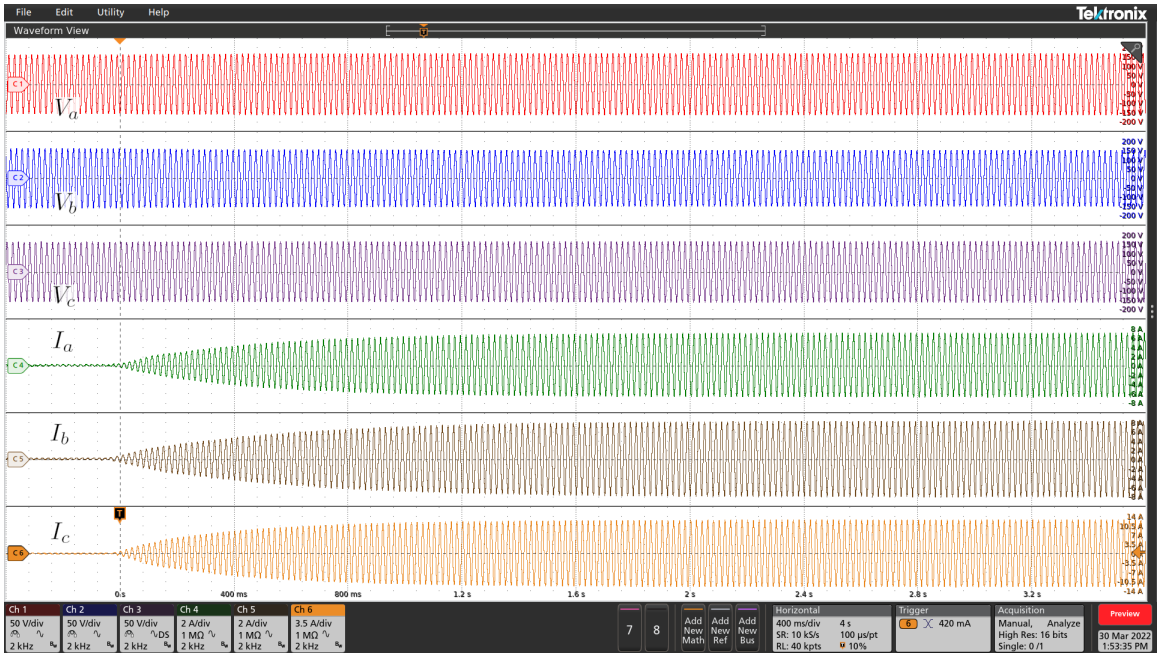

(b)

Figure 5-13: Grid tied inverter performing an active power step variation in a single phase. At $t = 0$ s the reference step changes $P_c^{\text{ref}} : 0 \rightarrow 1$ kW.

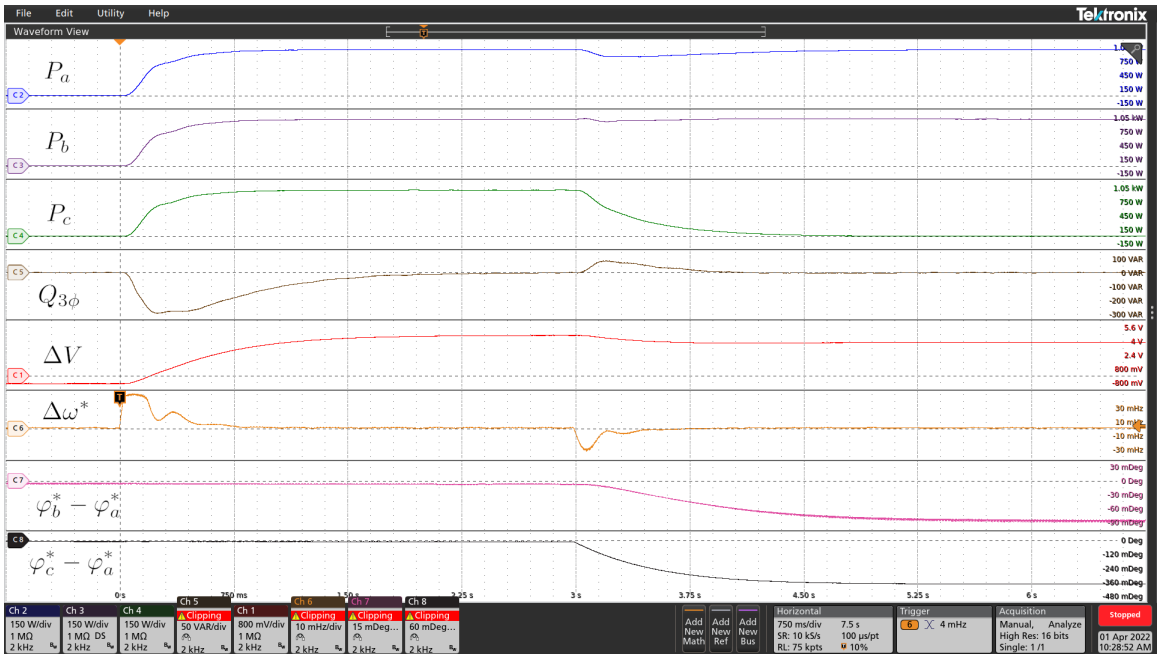

(a)

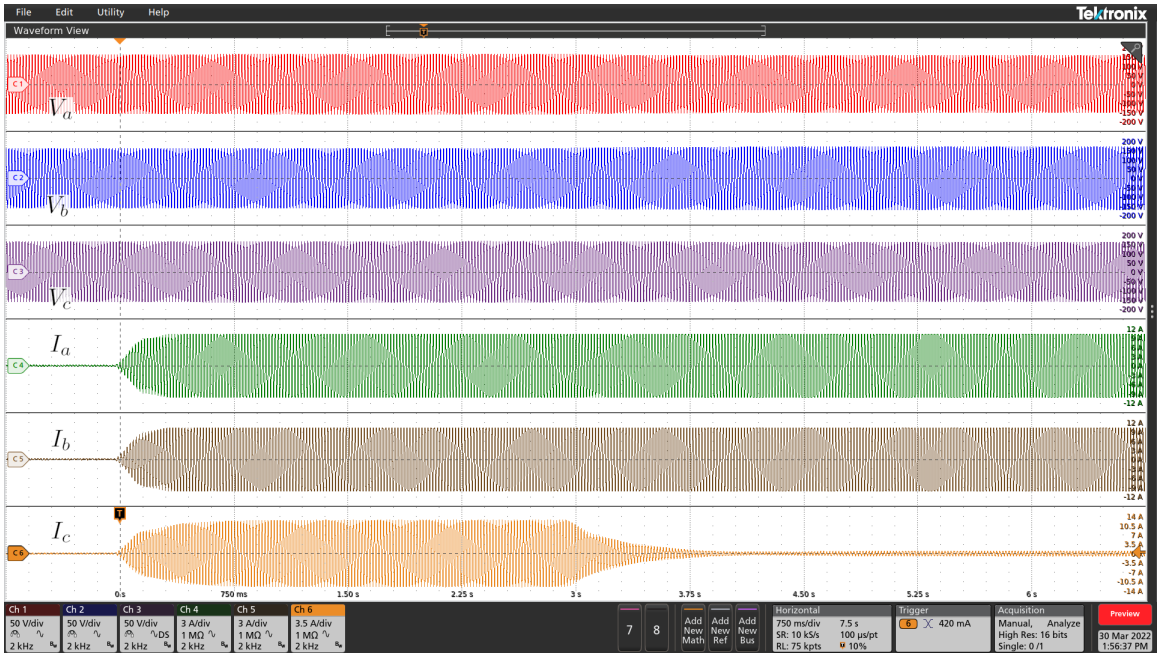

(b)

Figure 5-14: Grid tied inverter performing active power step variations. At $t = 0$ s the reference step changes $P^{\text{ref}}_{a,b,c} : 0 \rightarrow 1$ kW, then at $t = 3$ s $P^{\text{ref}}_{c} : 1\text{ kW} \rightarrow 0$.

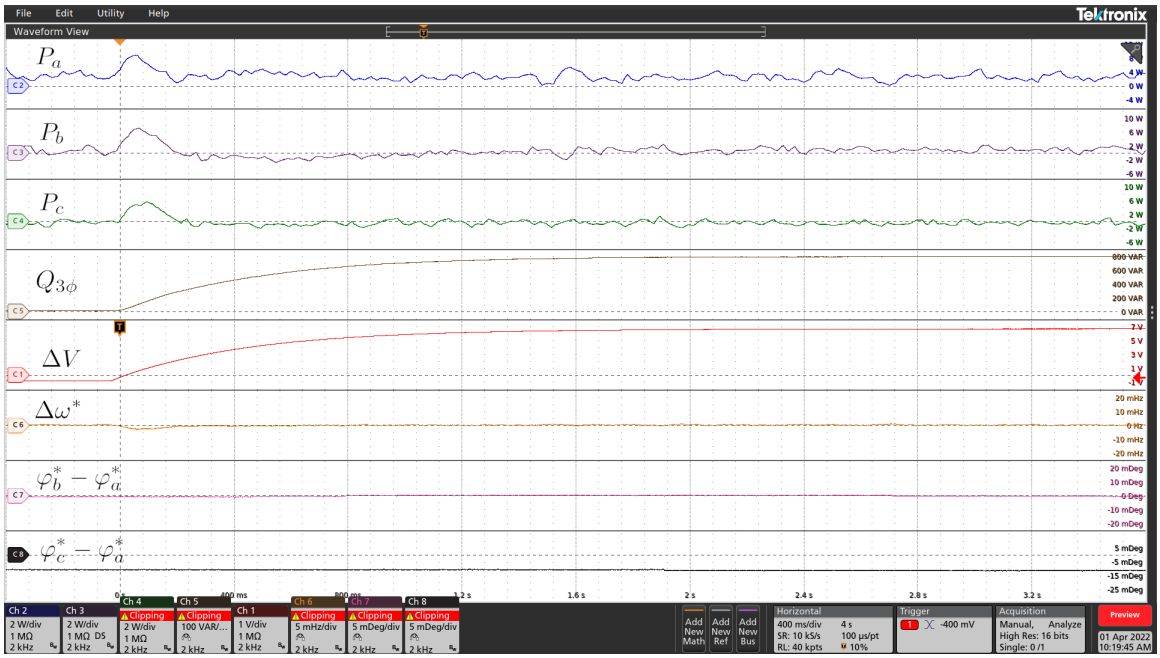

(a)

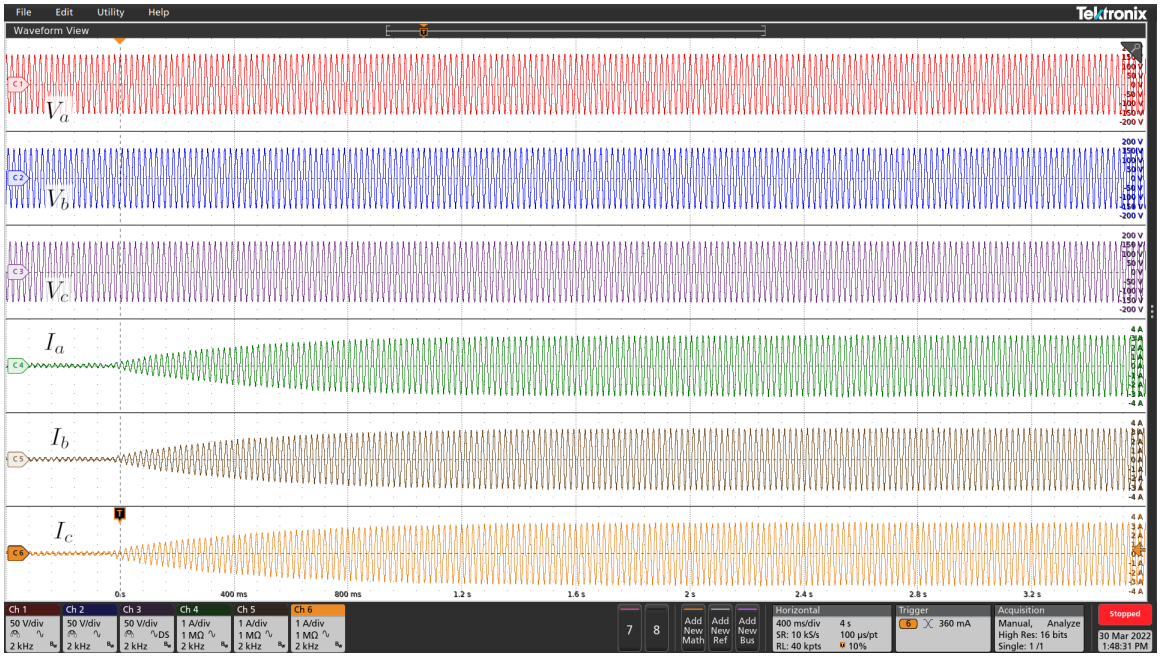

(b)

Figure 5-15: Grid tied inverter performing a reactive power step variation. At $t = 0$ s the reference step changes $Q_{3\phi}^{\text{ref}} : 0 \rightarrow 800$ VAr.

Supply of unbalanced load

As shown in Fig. 5-7, when an unbalanced load is connected to the grid, unbalanced currents start flowing. This causes two major problems: reactive power start flowing, causing distribution losses; moreover, the voltage drops on line impedances cause unbalances in grid voltages. This test is similar to the one performed in the aforementioned figure: a 50 Ω resistive load is connected between phases A and B. The inverter is employed to supply unbalanced per-phase active power while keeping its total active and reactive power regulated to zero. This allows the grid to inject balanced currents.

Transition towards island operation

In these tests, as before, an inverter is connected to the grid, which is realized by employing the remaining half-bridge modules. At some time instant, the grid is suddenly disconnected, and the inverter supplies the power needed by the load according to the droop laws.

In Fig. 5-17 a 50 Ω resistive load is connected to the grid together with the inverter. At $t = 0$ s the grid is disconnected. In (a) it is possible to notice grid voltage and frequency deviating from their nominal values, settling to a new value based on active and reactive power supplied to the load. Total reactive power is not zero because the output power is measured using average inductor current: this means that also current on the filter capacitors is taken into account. Supposing 110 V as RMS output voltage value and 50 Hz as grid frequency, then capacitors reactive power is $-3 \cdot 110^2 \cdot 2\pi 50 \cdot C_f \simeq -600$ VAr. In (b) it is possible to notice the quality of the voltage waveform during the transition. There is a minor voltage surge, due to the droop law, where the voltage amplitude is increased by 6%.

The test reported in Fig. 5-18 is the same as the previous one, with the difference that an unbalanced load is employed. Two 50 Ω and one 25 Ω resistors are connected together at one end, while at the other end the 25 Ω resistor is connected to phase C, while the other two are connected to phases A and B. In (b) it is possible to

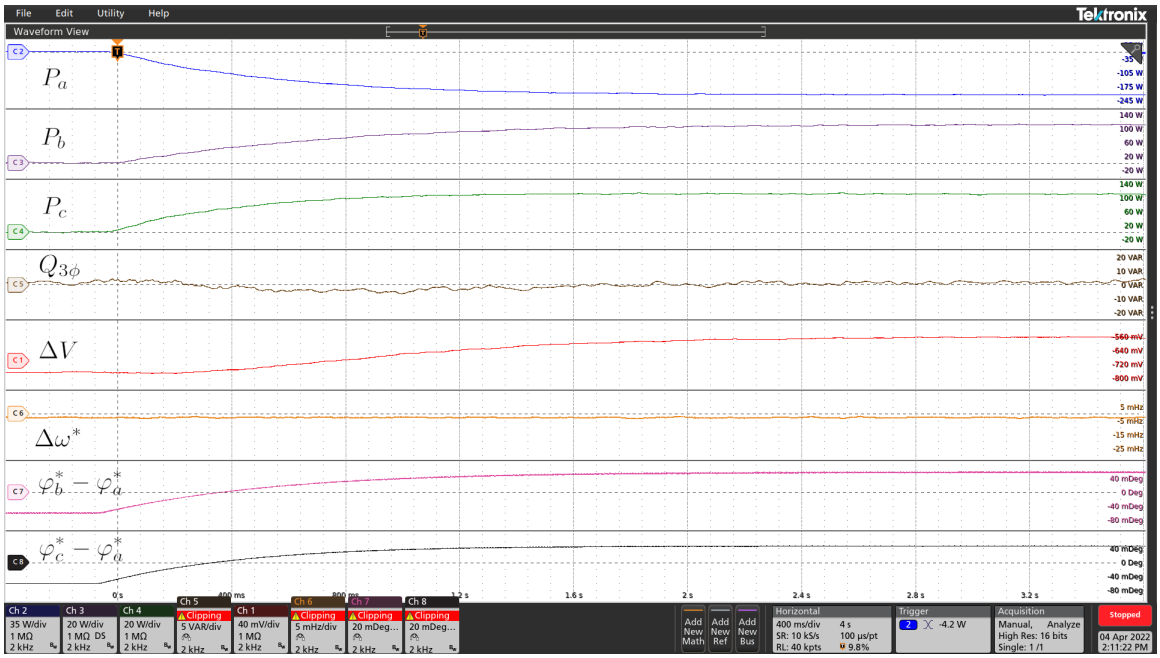

(a)

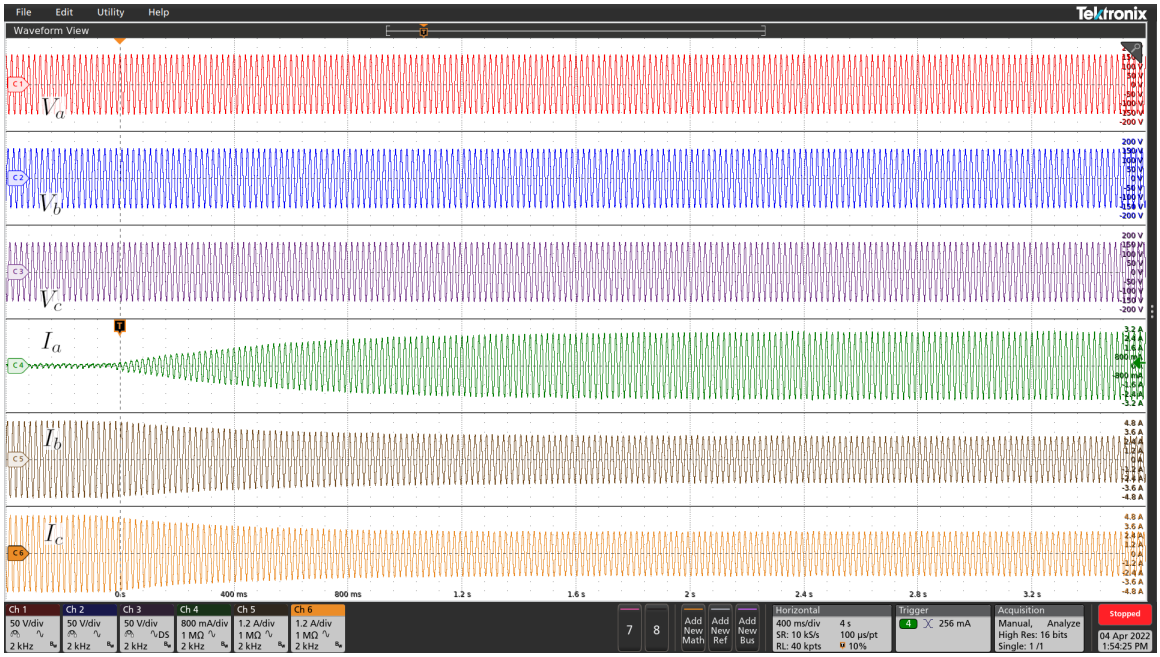

(b)

Figure 5-16: Inverter output power (a) and grid voltages and currents (b). The grid is initially supplying an unbalanced load. At $t = 0$ s the inverter injects unbalanced active power, while keeping total active and reactive power regulated to zero.

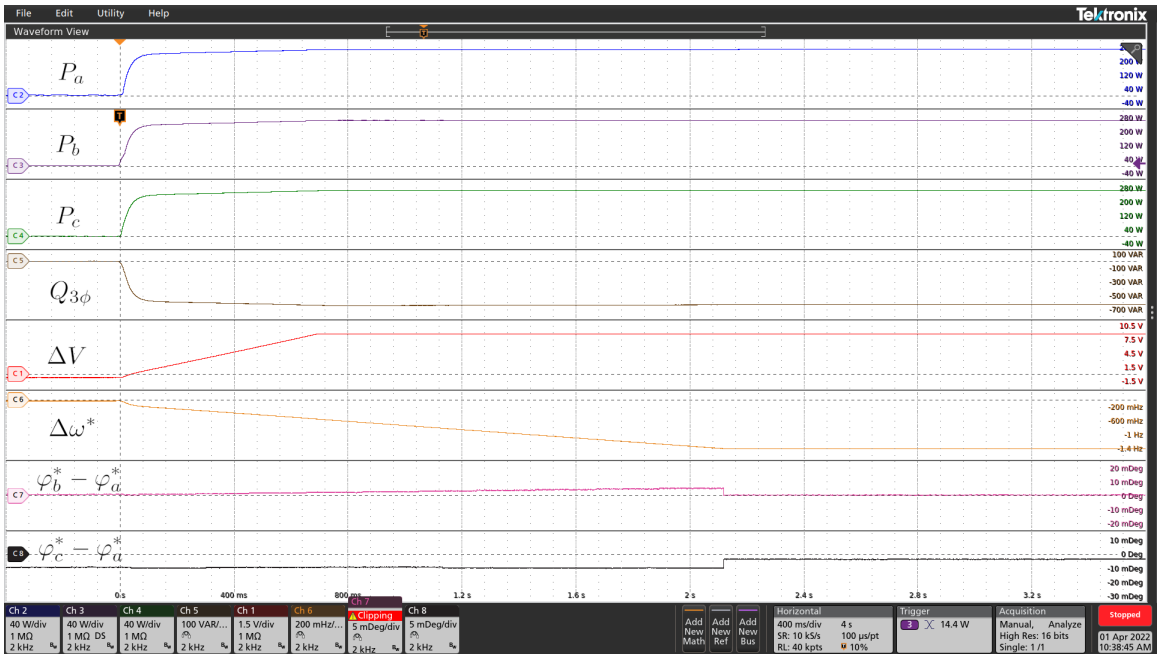

(a)

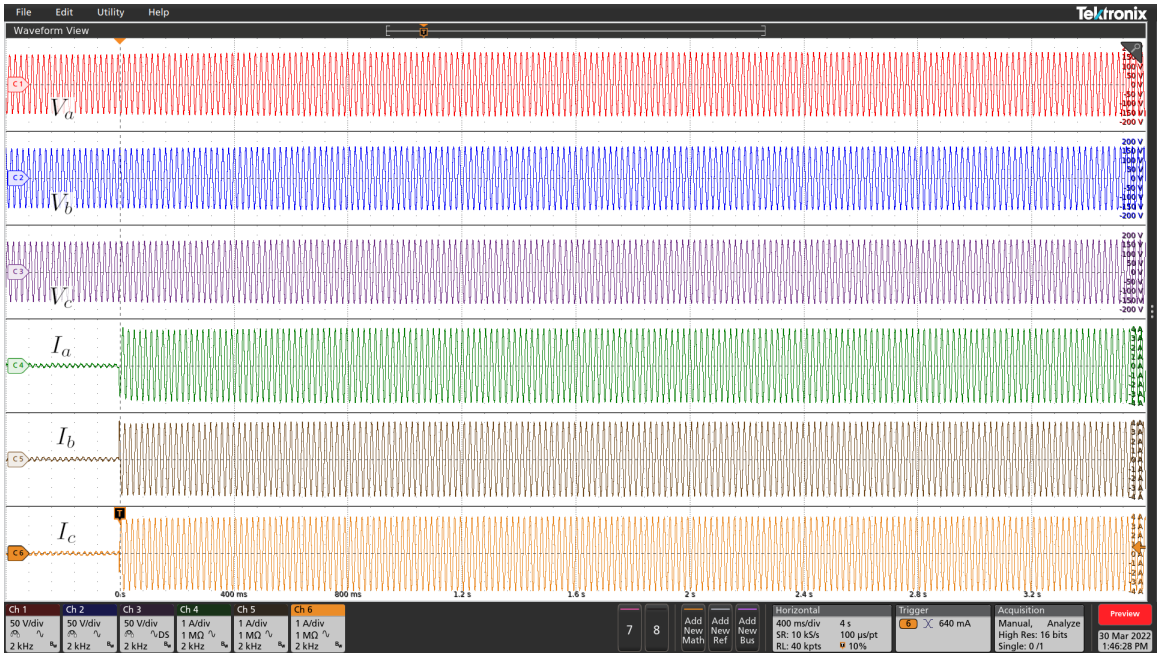

(b)

Figure 5-17: Transition toward island operation. At $t = 0$ s the grid is disconnected and the inverter supplies a balanced 50 Ω resistive load.

see some voltage sags and surges during the transition, which is completed at $t \simeq 1.7$ s. Voltage amplitude is initially increased until the point that the reactive power integrator saturates, where voltage amplitude reference settles at about 163 V. In the meanwhile, the per-phase power regulator tries to compensate for the power unbalance by acting on the per-phase angle, until the point in which the total active power integrator saturates (at $t \simeq 1.7$ s) and the per-phase regulator is turned off. During this process, the output current is affected and consequently voltage amplitude is subject to variations.

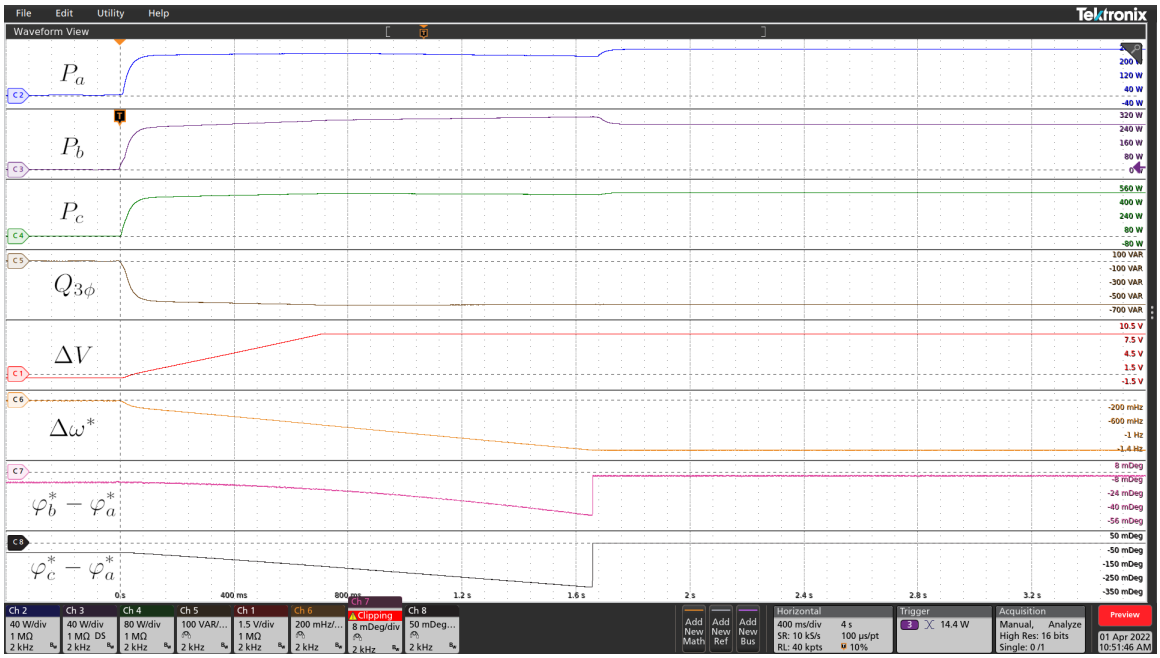

(a)

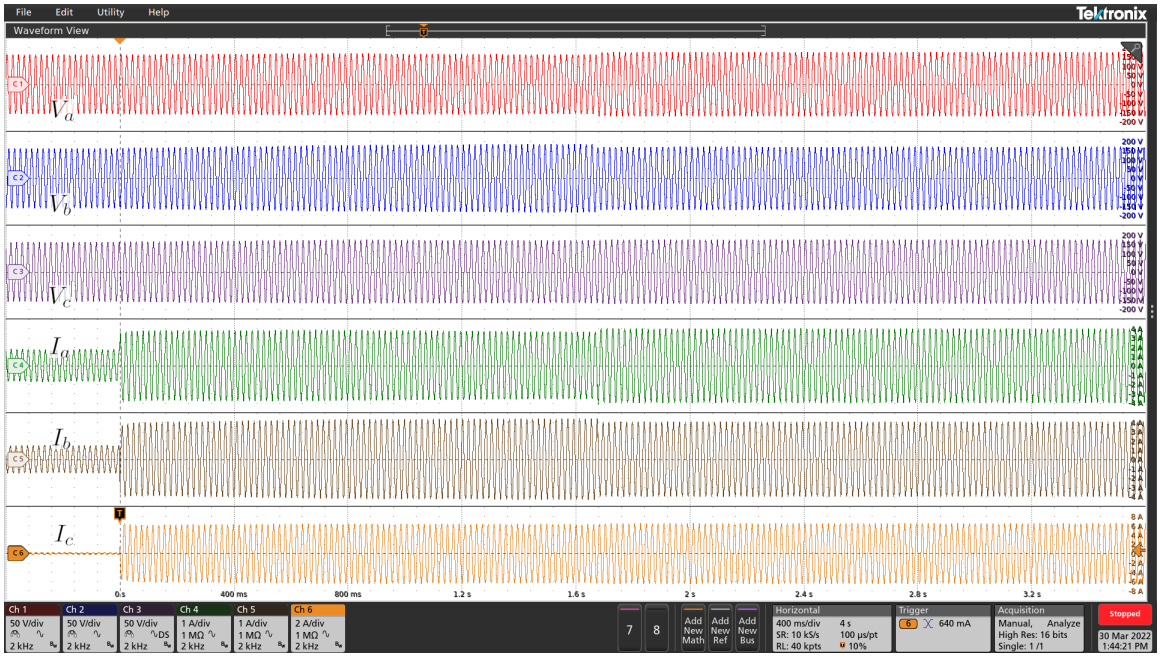

(b)

Figure 5-18: Transition toward island operation. At $t = 0$ s the grid is disconnected and the inverter supplies an unbalanced resistive load: two 50 Ω resistors with one end connected to phase A and B and a 25 Ω with one end connected to phase C. At the other end the three resistors are connected together.

Chapter 6

Conclusions

To overcome the challenges issued by the future energy scenario, current literature proposes several power controllers, each one with important features, addressing different specific needs, which may also result in opposing behaviors. The controller proposed herein, however, harmoniously integrates important features, offering a unique control system to face some of the modern issues in smart microgrids. Experimental tests have proven that per-phase control is capable of providing balanced power exchange with the grid when unbalanced loads are present, and in case of main grid failure, the transition toward island operation has proven to be smooth and practically seamless concerning the microgrid voltage, fulfilling expectations about this control scheme.

Considering the future development of the control, some considerations are reported in the following. Per-phase power control can be exploited by higher-level control structures to achieve various goals. The fact that this controller does not employ communication networks doesn't mean that it shouldn't be used: if the absence of critical communication networks (namely, communication networks without which the system can't operate) means higher reliability, the presence of uncritical communication may allow an optimized behavior of the microgrid. Distribution losses management, grid balancing, and other aspects can benefit from the presence of higher-level coordination of the converters supporting the microgrid and the power control flexibility given by the per-phase control considered in this thesis. The management of the

island condition can also benefit from higher-level coordination: droop parameters can be modified to optimize the behavior of the grid, both in terms of balance and power loss. Moreover, when at least one power converter operates according to droop law, another converter can indeed control their output power, allowing for example to modify per-phase output power to minimize grid unbalance.

Bibliography

[1] Hossein Abedini, Tommaso Caldognetto, and Paolo Mattavelli. "A Per-Phase Power Controller allowing Smooth Transitions to Islanded Operation". In: *2021 IEEE Energy Conversion Congress and Exposition (ECCE)*. 2021, pp. 973–979. DOI: 10.1109/ECCE47101.2021.9595168.

[2] Karel De Brabandere et al. "A Voltage and Frequency Droop Control Method for Parallel Inverters". In: *IEEE Transactions on Power Electronics* 22.4 (2007), pp. 1107–1115. DOI: 10.1109/TPEL.2007.900456.

[3] E. Espina, M. Espinoza, and R. Cárdenas. "Active power angle droop control per phase for unbalanced 4-wire microgrids". In: *2017 IEEE Southern Power Electron. Conf.* 2017, pp. 1–6. DOI: 10.1109/SPEC.2017.8333637.

[4] J. M. Guerrero et al. "Hierarchical Control of Droop-Controlled AC and DC Microgrids—A General Approach Toward Standardization". In: *IEEE Trans. Ind. Electron.* 58.1 (2011), pp. 158–172. DOI: 10.1109/TIE.2010.2066534.

[5] Wael A. Hashlamoun, Munther A. Hassouneh, and Eyad H. Abed. "New Results on Modal Participation Factors: Revealing a Previously Unknown Dichotomy". In: *IEEE Transactions on Automatic Control* 54.7 (2009), pp. 1439–1449. DOI: 10.1109/TAC.2009.2019796.

[6] Alexey B. Iskakov. "Definition of State-in-Mode Participation Factors for Modal Analysis of Linear Systems". In: *IEEE Transactions on Automatic Control* 66.11 (2021), pp. 5385–5392. DOI: 10.1109/TAC.2020.3043312.

[7] Stefano Lissandron and Paolo Mattavelli. "A controller for the smooth transition from grid-connected to autonomous operation mode". In: *2014 IEEE Energy Conversion Congress and Exposition (ECCE)*. 2014, pp. 4298–4305. DOI: 10.1109/ECCE.2014.6953987.

[8] I. J. Perez-arriaga, G. C. Verghese, and F. C. Schweppe. "Selective Modal Analysis with Applications to Electric Power Systems, PART I: Heuristic Introduction". In: *IEEE Transactions on Power Apparatus and Systems* PAS-101.9 (1982), pp. 3117–3125. DOI: 10.1109/TPAS.1982.317524.

[9] Joan Rocabert et al. "Control of Power Converters in AC Microgrids". In: *IEEE Transactions on Power Electronics* 27.11 (2012), pp. 4734–4749. DOI: 10.1109/TPEL.2012.2199334.

[10] Adrian Timbus et al. "Evaluation of Current Controllers for Distributed Power Generation Systems". In: *IEEE Trans. Power Electron.* 24.3 (2009), pp. 654–664. DOI: 10.1109/TPEL.2009.2012527.

[11] Wei Yao et al. "Design and Analysis of the Droop Control Method for Parallel Inverters Considering the Impact of the Complex Impedance on the Power Sharing". In: *IEEE Transactions on Industrial Electronics* 58.2 (2011), pp. 576–588. DOI: 10.1109/TIE.2010.2046001.